UNBOUNDED SETS OF ATTRACTION[*]

GIAN-ITALO BISCHI[†]
Istituto di Scienze Economiche, University of Urbino, 61029 Urbino, Italy

CHRISTIAN MIRA[‡]
19 rue d'Occitanie, Fonsegrives 31130 Quint,
MIDIVAL, 2 rue Camichel, 31071 Toulouse Cedex, France

LAURA GARDINI[§]
Istituto di Matematica "Levi", University of Parma, Italy
and Istituto di Scienze Economiche, University of Urbino 61029 Urbino, Italy

In this paper we show that unbounded chaotic trajectories are easily observed in the iteration of maps which are not defined everywhere, due to the presence of a denominator which vanishes in a zero-measure set. Through simple examples, obtained by the iteration of one-dimensional and two-dimensional maps with denominator, the basic mechanisms which are at the basis of the existence of unbounded chaotic trajectories are explained. Moreover, new kinds of contact bifurcations, which mark the transition from bounded to unbounded sets of attraction, are studied both through the examples and by general theoretical methods. Some of the maps studied in this paper have been obtained by a method based on the Schröder functional equation, which allows one to write closed analytical expressions of the unbounded chaotic trajectories, in terms of elementary functions.

1. Introduction

The literature on chaotic dynamical systems mainly concerns bounded attracting sets, while unbounded trajectories are usually considered as synonymous of diverging trajectories. Also the definitions of attractor given in the current literature are almost all referred to compact sets (see e.g. [Robinson, 1995; Katok & Hasselblatt, 1995; Wiggins, 1990]). The fact that this may be a restrictive point of view has been recently emphasized by some authors. For example [Brown & Chua, 1996] write "... in defining chaos, no restrictions as to boundedness is reasonable".

Indeed, unbounded chaotic trajectories naturally arise in the iteration of maps with a denominator which can vanish. For example, the existence of a "nonbounded chaotic solution" in a one-dimensional recurrence with denominator, has been shown in [Mira, 1982] (see also [Mira *et al.*, 1996a, p. 38]).

The main purpose of this paper is to show examples of unbounded chaotic trajectories and to describe some nonclassical (or contact) bifurcations which cause the transition from bounded asymptotic dynamics to unbounded (but not diverging) dynamics, both in one-dimensional and

---

two-dimensional fractional maps. The basic feature of an unbounded and not diverging trajectory is that points of arbitrarily large norm may belong to the trajectory, but they do not give rise to divergence, i.e. these points have images of smaller norm. Of course, this property may cause some difficulties in the numerical iteration of a map by a computer, since an overflow error may occur even if the numerically generated trajectory is not diverging. Furthermore, the occurrence of such a numerical error may be strongly dependent on the kind of computer or the kind of floating-point arithmetic used to perform the calculations. For this reason, even if we give some numerical representations of unbounded sets of attraction in order to help the reader to visualize the objects we are studying, we avoid using just computer experiments in order to prove the existence of such kinds of trajectories. Indeed, in the examples we give in this paper, we show the existence of unbounded chaotic trajectories on the basis of theoretical arguments, and in some cases we even give the closed analytical expression of such trajectories in terms of elementary algebraic and transcendental functions.

The results of this paper are partially based on the studies published in a previous paper by the same authors, concerning the properties of two-dimensional maps which are not defined in the whole plane, due to the vanishing of a denominator (see [Bischi *et al.*, 1999a]), and on some studies on chaotic recurrences with analytic solutions obtained by a method based on the Schröder functional equation, published in [Mira, 1982] (see also [Gumowski & Mira, 1980] or [Mira *et al.*, 1996a]).

The plan of the paper is the following. In Sec. 2 we introduce the concept of *set of nondefinition*, δ_s, for both one-dimensional and two-dimensional maps, and some consequences of the presence of δ_s on the geometrical properties of the maps are investigated. In Sec. 3 we propose some simple one-dimensional maps whose iteration generates unbounded chaotic sequences, and through these examples we try to explain the basic mechanisms and bifurcations leading to the creation of *Unbounded Sets of Attraction*. We show that unbounded chaotic sets can be easily observed in the iteration of one-dimensional maps characterized by the presence of a vertical asymptote, the abscissa of which cancels the map's denominator. A simple one-dimensional noninvertible map with denominator is proposed in order to show how the transition from bounded asymptotic dynamics to Unbounded

Sets of Attraction can be explained as the effect of nonclassical bifurcations, due to a contact between a critical point and a vertical asymptote. In Sec. 3 we also propose a one-dimensional recurrence with unbounded chaotic dynamics, whose solutions can be written in closed form, expressed in terms of elementary functions. In Sec. 4 we generalize some of these concepts to two-dimensional recurrences. For many purposes, a curve where a denominator vanishes may be considered as a two-dimensional analogue of a vertical asymptote, and the creation of two-dimensional unbounded chaotic sets in noninvertible maps may be caused by a contact between δ_s and critical curves.

The study of such peculiar dynamical behaviors of maps with denominator has been motivated by practical reasons, because discrete dynamical systems, obtained by the iteration of maps with denominator, are often seen in applications. For example, many iterative methods to find numerical solutions of equations, based on the well known Newton method, are expressed by recurrences with a denominator which can vanish (see e.g. [Curry *et al.*, 1983; Billings & Curry, 1996; Billings *et al.*, 1998; Gardini *et al.*, 1999]) as well as implicit methods for the numerical solution of differential equations [Yee & Sweby, 1994]. Moreover, some discrete-time dynamical systems used to model the evolution of economic and financial systems, which are often expressed by implicit recurrences $F(x_n, x_{n+1}) = 0$, assume the form of recurrences with denominator when they are expressed as $x_{n+1} = f(x_n)$ (see e.g. [Marimon & Sunder, 1994; Bischi & Naimzada, 1997]).

2. The Set of Nondefinition and Related Properties

In this paper we consider one-dimensional and two-dimensional fractional maps which are, respectively, not defined in a subset of the real line or of the plane, due to the vanishing of some denominator.

The one-dimensional maps considered in this paper are of the form

$$x \rightarrow x' = f(x) \quad \text{with} \quad f(x) = \frac{N(x)}{D(x)} \qquad (1)$$

where $N(x)$ and $D(x)$ are functions of the real variable x which are assumed to be continuous in $\mathbb{R}$. The *set of nondefinition* for the map (1) is given by

the set of points in which the denominator vanishes

$$\delta_s = \{x \in \mathbb{R} | D(x) = 0\}. \tag{2}$$

We assume that δ_s is a set of isolated points of $\mathbb{R}$. The iteration of the map (1) is well defined provided that the initial condition belongs to the set E given by

$$E = \mathbb{R} \setminus \Lambda \tag{3}$$

where Λ is the union of the preimages of any rank of the set of nondefinition

$$\Lambda = \bigcup_{k=0}^{\infty} f^{-k}(\delta_s) \tag{4}$$

where $f^{-k}(\delta_s)$ denotes the set of the rank-k preimages of δ_s, i.e. the set of points which are mapped into δ_s after k applications of f ($f^0(\delta_s) \equiv \delta_s$). From the definition (3) it follows that E is a *trapping set* for the map f, i.e. $f(E) \subseteq E$, so that the iteration of the restriction

$$f : E \to E$$

generates nonterminated trajectories. From the assumption that δ_s is a set of isolated points it follows that the set Λ defined in (4) has zero Lebesgue measure in $\mathbb{R}$, so that it makes sense to consider the restriction of f to E.

The two-dimensional maps considered in this paper are of the form

$$(x, y) \to (x', y') = T(x, y) = (T_1(x, y), T_2(x, y)) \tag{5}$$

with

$$T_1(x, y) = \frac{N_1(x, y)}{D_1(x, y)} \quad \text{or} \quad T_2(x, y) = \frac{N_2(x, y)}{D_2(x, y)}$$

where "or" means *at least one*. The functions $N_i(x, y)$ and $D_i(x, y)$, $i = 1, 2$, are assumed to be continuous in the whole plane $\mathbb{R}^2$. Hence, the *set of nondefinition* of (5) is given by the set of points where at least one denominator vanishes

$$\delta_s = \{(x, y) \in \mathbb{R}^2 | D_1(x, y) = 0 \quad \text{or} \quad D_2(x, y) = 0\} \tag{6}$$

and we assume that it is formed by the union of smooth curves of the plane. Following arguments similar to those given for the one-dimensional case, in order to have a well defined recurrence by the iteration of T we shall consider its restriction to the trapping set E defined as

$$E = \mathbb{R}^2 \setminus \Lambda \tag{7}$$

where Λ is given by

$$\Lambda = \bigcup_{k=0}^{\infty} T^{-k}(\delta_s) \tag{8}$$

and $T^{-k}(\delta_s)$ denotes the set of the rank-k preimages of δ_s, i.e. the set of points which are mapped into δ_s after k applications of T ($T^0(\delta_s) \equiv \delta_s$). Also in this case, from the assumption that δ_s is a set of curves it follows that the set Λ defined in (8) has zero Lebesgue measure in $\mathbb{R}^2$. We shall consider the recurrences obtained by the iteration of the restriction of (5) to E, i.e.

$$T : E \to E.$$

Both for the one-dimensional and the two-dimensional fractional maps, the presence of a nonempty set δ_s implies that the map may transform bounded subsets of E into unbounded sets. This property is trivial in the case of one-dimensional maps (1). In fact, let us consider a compact interval $I = [a, b]$ such that $I \cap \delta_s = \emptyset$. Being $N(x)$ and $D(x)$ continuous functions, and $D(x) \neq 0$ for each $x \in I$, the image $f(I)$ is a compact interval. Instead, if $I \cap \delta_s$ contains at least one point $x_0 \in [a, b]$ and if $N(x_0) \neq 0$, then the image by f of any neighborhood of x_0, deprived of x_0, includes one or two unbounded intervals.

A similar reasoning applies to the case of two-dimensional fractional maps (5). Consider first a bounded curve segment γ such that $\gamma \cap \delta_s = \emptyset$, so that the map T is continuous for all the points of γ. Since γ is a compact subset of $\mathbb{R}^2$, its image $T(\gamma)$ is also compact.

Now, let us consider a bounded and smooth simple arc γ which crosses an arc belonging to the set of nondefinition δ_s, say $\gamma \cap \delta_s = \{(x_0, y_0)\}$. We study how γ is transformed by the application of the map T, i.e. what is the shape of its image $T(\gamma)$. On taking the image $T(\gamma)$, we assume that the arc γ is deprived of the point (x_0, y_0) in which it intersects δ_s. Let us assume that in a neighborhood of (x_0, y_0) γ is represented by the parametric equations

$$\gamma(\tau) : \begin{cases} x(\tau) = x_0 + \xi_1\tau + \xi_2\tau^2 + \cdots \\ y(\tau) = y_0 + \eta_1\tau + \eta_2\tau^2 + \cdots \end{cases} \quad \tau \neq 0 \tag{9}$$
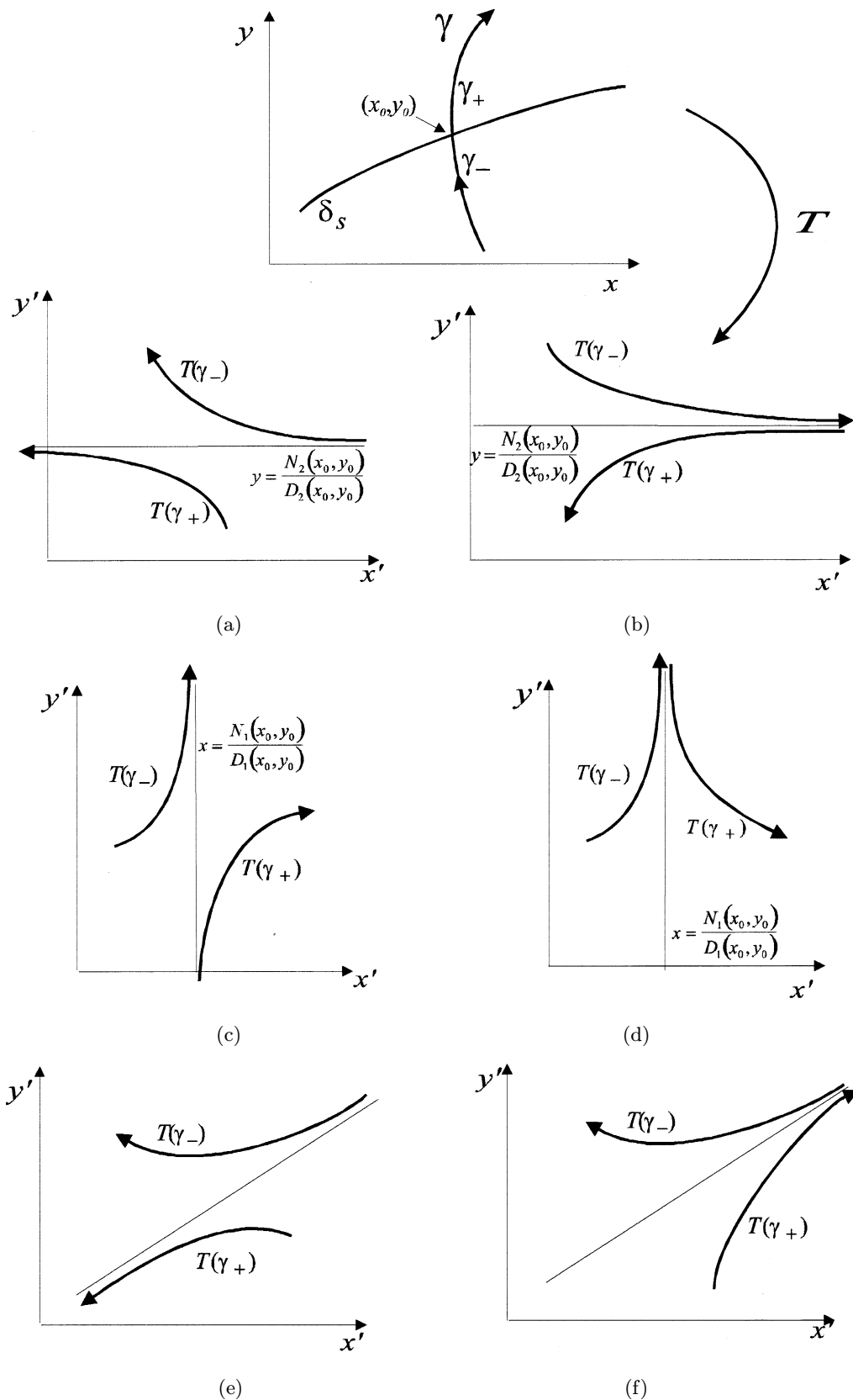
Fig. 1. Qualitative sketches to describe how an arc γ, which crosses the set of nondefinition δ_s, is transformed by an application of the map (5). (a) Only the denominator D_1 vanishes, and changes its sign, crossing the arc of δ_s shown in the upper part of the figure. (b) Only the denominator D_1 vanishes along the arc of δ_s, but it does not change its sign as γ crosses δ_s. (c) Only the denominator D_2 vanishes, and changes its sign, crossing the arc of δ_s. (d) Only the denominator D_2 vanishes along the arc of δ_s, but it does not change its sign as γ crosses δ_s. (e) and (f) Both the denominators D_1 and D_2 vanish along the arc of δ_s.

1440

The portion of γ in such a neighborhood can be seen as the union of two disjoint pieces, say $\gamma = \gamma_- \cup \gamma_+$, where γ_- and γ_+ denote the portions of γ located on opposite sides with respect to the arc of δ_s, obtained from (9) with $\tau < 0$ and $\tau > 0$ respectively. The closure $\overline{\gamma(\tau)}$ is such that $\overline{\gamma_-}(0) = \overline{\gamma_+}(0) = (x_0, y_0)$ (see Fig. 1). As $(x_0, y_0) \in \delta_s$ we have, according to the definition (6) of δ_s, $D_1(x_0, y_0) = 0$ or $D_2(x_0, y_0) = 0$ or both.

If only D_1 vanishes in (x_0, y_0) and the corresponding numerator $N_1(x_0, y_0) \neq 0$ then we have

$$\lim_{\tau \to 0} T(\gamma(\tau)) = \left(\infty, \frac{N_2(x_0, y_0)}{D_2(x_0, y_0)}\right) \qquad (10)$$

where ∞ means either $+\infty$ or $-\infty$. This means that the image $T(\gamma)$ is made up of two disjoint unbounded arcs asymptotic to the horizontal line of equation

$$y = \frac{N_2(x_0, y_0)}{D_2(x_0, y_0)} \qquad (11)$$

If the denominator $D_1(x, y)$ changes sign as the point (x, y) crosses δ_s, moving along the arc γ, then the two unbounded branches of $T(\gamma)$ are asymptotic to the line (11) as in Fig. 1(a), otherwise a situation like the one shown in Fig. 1(b) is obtained.

Analogously, if only D_2 vanishes in (x_0, y_0) and the corresponding numerator $N_2(x_0, y_0) \neq 0$ then we have

$$\lim_{\tau \to 0} T(\gamma(\tau)) = \left(\frac{N_1(x_0, y_0)}{D_1(x_0, y_0)}, \infty\right) \qquad (12)$$

so that the image $T(\gamma)$ is made up of two disjoint unbounded arcs asymptotic to the vertical line of equation

$$x = \frac{N_1(x_0, y_0)}{D_1(x_0, y_0)}. \qquad (13)$$

If the denominator $D_2(x, y)$ changes sign as the point (x, y) crosses δ_s, moving along the arc γ, then the two unbounded branches of $T(\gamma)$ are asymptotic to the line (13) as in Fig. 1(c), otherwise a situation like the one shown in Fig. 1(d) is obtained.

Finally, if both the denominators D_1 and D_2 vanish in (x_0, y_0), and the corresponding numerators $N_i(x_0, y_0) \neq 0$, $i = 1, 2$, then we have

$$\lim_{\tau \to 0} T(\gamma(\tau)) = (\infty, \infty) \qquad (14)$$

so that the image $T(\gamma)$ is made up of two disjoint unbounded arcs asymptotic to a line of slope

$$m = \frac{N_2(x_0, y_0)}{N_1(x_0, y_0)} \lim_{\tau \to 0} \frac{D_1(x(\tau), y(\tau))}{D_2(x(\tau), y(\tau))} \qquad (15)$$

[see Figs. 1(e) and 1(f)].

In the particular case in which both a denominator and the corresponding numerator vanish in $(x_0, y_0) \in \delta_s$, so that forms of the type $0/0$ are seen in the limits given above, we may have bounded images $T(\gamma)$ of an arc γ crossing δ_s in (x_0, y_0). In this case the point (x_0, y_0) is called *focal point* (see [Bischi *et al.*, 1999a]). In order to see the difference between a focal point and a nonfocal point of δ_s, let us consider different arcs γ_i which cross an arc of δ_s, as in Fig. 2. We assume, without loss of generality, that along the considered arc of δ_s only $D_2(x, y)$ vanishes. The arcs γ_1 and γ_3 cross through δ_s at the nonfocal points (x_1, y_1) and (x_3, y_3), such that $D_2(x_1, y_1) = 0$ and $D_2(x_3, y_3) = 0$ with $N_1(x_1, y_1) \neq 0$ and $N_1(x_3, y_3) \neq 0$, whereas the point (x_2, y_2) is assumed to be a focal point, that is, it satisfies $D_2(x_2, y_2) = N_2(x_2, y_2) = 0$. Of course, analogous situations are obtained for arcs of δ_s where only D_1, or both D_1 and D_2, vanish,

(a)

(b)
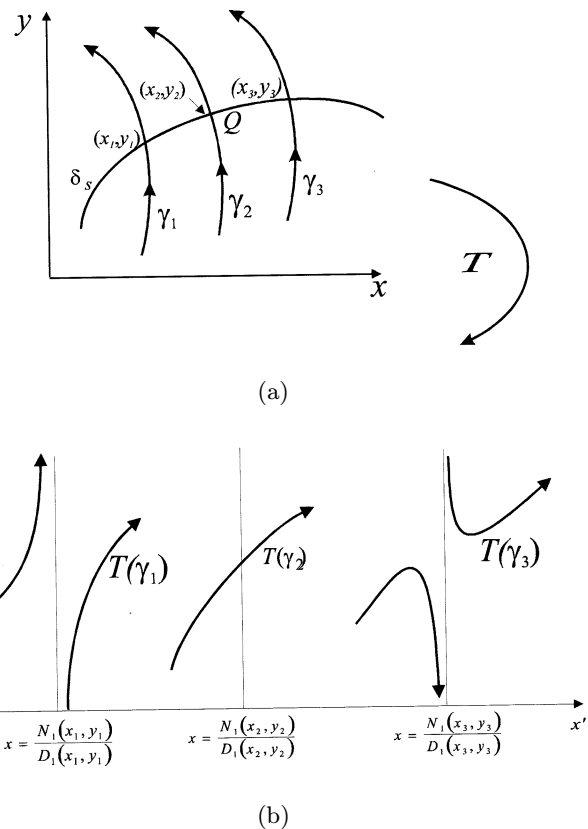
Fig. 2. Qualitative representation of the images of three different arcs γ_i, $i = 1, 2, 3$, such that γ_1 and γ_3 cross the set of nondefinition δ_s at points where only D_2 vanishes, and $N_2 \neq 0$ whereas γ_2 crosses δ_s at a *focal point*, denoted by Q, where both N_2 and D_2 vanish. In (a) the three arcs γ_i are represented, and the corresponding images $T(\gamma_i)$ are shown in (b).

corresponding to the cases of horizontal and oblique asymptotes respectively.

From these results it is immediate to deduce that a contact between a bounded curve segment γ and an arc of δ_s may cause noticeable qualitative changes in the shape of the image $T(\gamma)$. As shown in [Bischi et al., 1999a] these contacts may be particularly important when the segments of curves considered are portions of phase curves of the map T, such as *invariant closed curves* as well as *unstable sets* of saddle fixed points or saddle cycles. In these cases the contacts with δ_s can cause the occurrence of new types of global bifurcations, specific to maps with a vanishing denominator, that may change the structure of the attracting sets or of their basins (see [Bischi et al., 1997, 1999a]).

In this paper we shall focus our attention on the bifurcations leading to the creation of unbounded sets of attraction, related to a contact between an attractor and δ_s.

To understand the geometric and dynamic properties of fractional maps, which are at the basis of such bifurcations, we describe now what happens to the image of a bounded curve segment γ when it has a tangential contact with δ_s and subsequently crosses it at two points. Again, we assume, without loss of generality, that only $D_2(x, y)$ vanishes along the arc of δ_s considered. If γ lies entirely in a region in which no denominator of the map T vanishes, so that the map is continuous at all the points of γ, then also its image $T(\gamma)$ is a bounded curve, as qualitatively shown in the two sketches of Fig. 3(a). We now imagine to move γ towards δ_s, until it becomes tangent to it at a point $P_0 = (x_0, y_0)$ which is not a focal point. This implies that the image $T(\gamma)$ is given by the union of two disjoint and unbounded branches, both asymptotic to the line σ of equation $x = N_1(x_0, y_0)/D_1(x_0, y_0)$. In Fig. 3(b) two possible situations, which may be seen as possible evolutions of the two arcs $T(\gamma)$ of Fig. 3(a), are qualitatively represented. At the tangential contact between γ and δ_s we have $T(\gamma) = T(\gamma_a) \cup T(\gamma_b)$, where γ_a and γ_b are the two portions of γ separated by the point $P_0 = \gamma \cap \delta_s$. For P_0 the map T is not defined and the limit of $T(x, y)$ assumes the form (12) as $(x, y) \to P_0$ along γ_a, as well as along γ_b. In such a situation any image of γ of rank $k > 1$, given by $T^k(\gamma)$, includes two disjoint unbounded branches, asymptotic to the rank-k image of the line σ, $T^k(\sigma)$.

As γ continues to move so that it crosses δ_s at two points, say $P_1 = (x_1, y_1)$ and $P_2 =$

(x_2, y_2), both nonfocal points, then the asymptote σ splits into two disjoint asymptotes σ_1 and σ_2 of equations $x = N_1(x_1, y_1)/D_1(x_1, y_1)$ and $x = N_1(x_2, y_2)/D_1(x_2, y_2)$ respectively, and the image $T(\gamma)$ is given by the union of three disjoint unbounded branches, $T(\gamma) = T(\gamma_a) \cup T(\gamma_c) \cup T(\gamma_b)$, where γ_a, γ_b and γ_c are the three portions of γ separated by the two points P_1 and P_2 at which the denominator vanishes. In Fig. 3(c) some

(a)

(b)

(c)
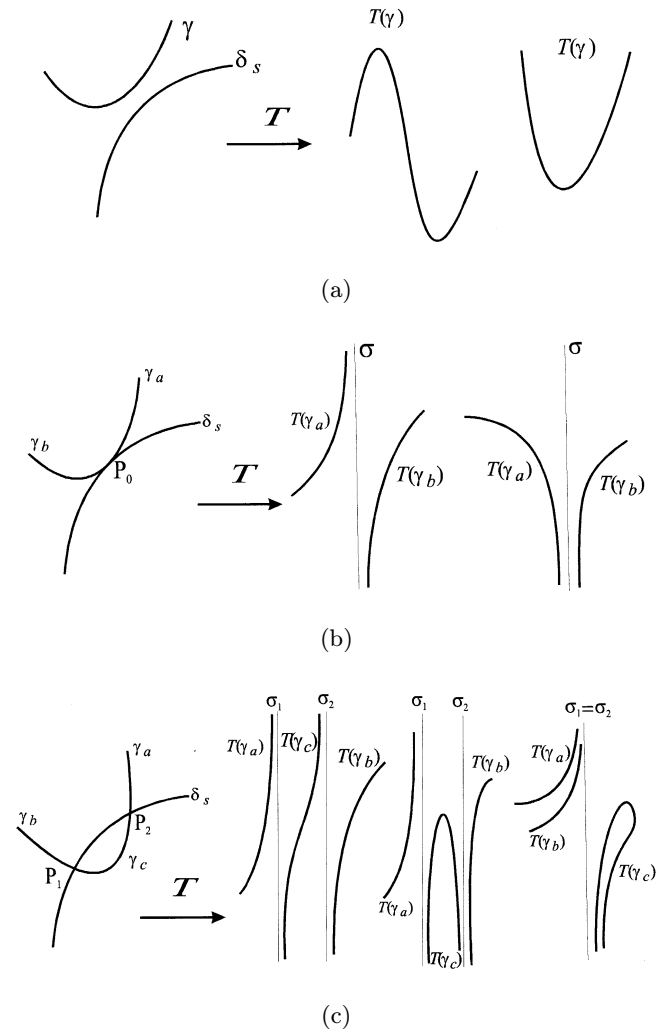
Fig. 3.   Qualitative sketches to show how the image of an arc γ changes when the arc moves until it has a tangential contact with δ_s and then crosses it at two points. The arc γ and the curve of nondefinition δ_s are shown on the left, the corresponding images on the right. Only the denominator D_2 is assumed to vanish along δ_s. (a) $\gamma \cap \delta_s = \emptyset$: $T(\gamma)$ is a compact curve (two different situations are shown) (b) $\gamma \cap \delta_s = P_0$: $T(\gamma)$ is formed by two unbounded branches, asymptotic to the line $x = N_1(P_0)/D_1(P_0)$. Two different situations are shown, possible evolutions of the two situations shown in (a). (c) $\gamma \cap \delta_s = \{P_1, P_2\}$: $T(\gamma)$ is formed by three unbounded branches, asymptotic to the lines $x = N_1(P_1)/D_1(P_1)$ and $x = N_1(P_2)/D_1(P_2)$. Three different situations are shown.

different possible shapes of $T(\gamma)$ are qualitatively shown, according to the sign of the denominator $D_2(x, y)$ along the curve γ (i.e. whether $D_2(x, y)$ changes the sign or not, or whether $N_2(P_1)$ and $N_2(P_2)$ have the same sign or not). Of course, also the image of γ of rank $k > 1$, $T^k(\gamma)$, includes three disjoint unbounded arcs, asymptotic to the curves $T^k(\sigma_1)$ and $T^k(\sigma_2)$, rank-k images of σ_1 and σ_2 respectively.

The qualitative change of $T(\gamma)$, due to a contact between γ and δ_s, may represent an important contact bifurcation of a fractional map T when γ is, for example, the unstable set W^u of a saddle point or saddle cycle. In fact, if A is an attracting set and $p \in A$ denotes a point of A, then the whole unstable set of p is necessarily included in A, i.e. $W^u(p) \subseteq A$. Hence, if $W^u(p)$ includes unbounded branches, due to a crossing with δ_s, then also A must necessarily be unbounded. In the following sections we show many examples of such unbounded attracting sets, both in one-dimensional and two-dimensional maps.

3. One-Dimensional Examples

3.1. *A simple recurrence with an unbounded chaotic set*

Let us consider the recurrence $x_{n+1} = f(x_n)$, where f is the fractional rational map

$$x' = f(x) = \frac{x^2 - 1}{2x + 1}. \tag{16}$$

For this map, the set of nondefinition is $\delta_s = \{-1/2\}$. So, the recurrence is well defined provided that the initial condition x_0 belongs to the set $E = \mathbb{R} \setminus \Lambda$, where Λ is defined as

$$\Lambda = \bigcup_{k=0}^{\infty} f^{-k}\left(-\frac{1}{2}\right).$$

At $x = -1/2$, where the denominator of (16) vanishes, the graph of the map has a vertical asymptote. Moreover, for large values of $|x|$ the graph approaches an asymptote of equation $x' = \frac{1}{2}x - \frac{1}{4}$ (see Fig. 4). The shape of the graph of (16) gives us an intuitive understanding of the mechanism which is at the basis of the existence of an unbounded chaotic set. In fact, points arbitrarily close to $x = -1/2$ have images of arbitrarily large modulus (close to infinity) and the iterated images of points very far from the origin have images of smaller and smaller modulus, because for large values of $|x|$ the
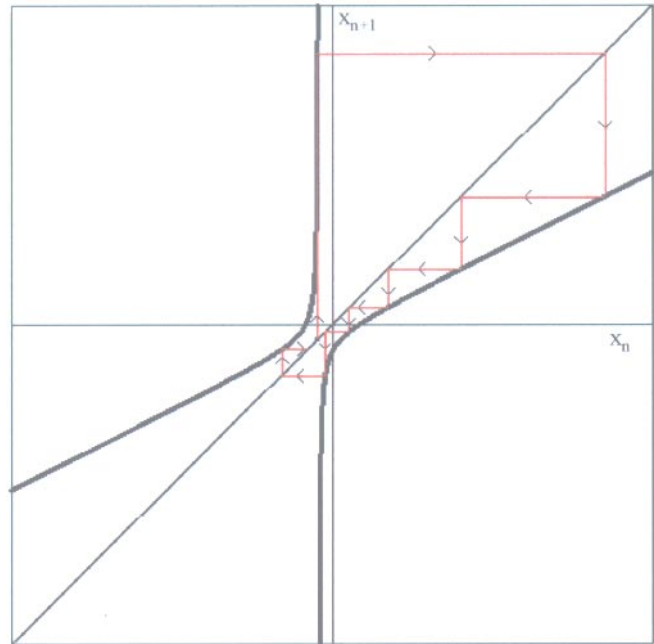
Fig. 4. Graph of the map (16) together with the early iterates of a typical trajectory, shown by the König–Lemeray staircase diagram.

map (16) is approximated by the linear contraction $x' = \frac{1}{2}x - \frac{1}{4}$. So, starting from arbitrarily large values of $|x|$, smaller values are obtained by the iteration of f, until x approaches the value $x = -1/2$, so that large values are obtained again, and so on.

Indeed, it is easy to prove that the iteration of the map (16) generates chaotic trajectories. In fact, (16) is conjugate to the map

$$z' = s(z) = \begin{cases} 2z & \text{for} \quad 0 \le z \le \frac{1}{2} \\ 2z - 1 & \text{for} \quad \frac{1}{2} < z \le 1 \end{cases} \tag{17}$$

by the conjugacy transformation (see [Billings *et al.*, 1997])

$$z = h(x) = \frac{1}{2} + \frac{1}{\pi}\arctan\frac{2x + 1}{\sqrt{3}}. \tag{18}$$

The dynamics of (17) are well known, from both a topological and a measure theoretical point of view: It has chaotic dynamics in the interval $[0, 1]$ with an absolutely continuous invariant ergodic measure associated with it. Hence the fractional map (16) has chaotic dynamics in the unbounded interval $(-\infty, +\infty)$ with an absolutely continuous invariant measure on it. It can be noticed that the map (17)

(a)

(b)

(c)
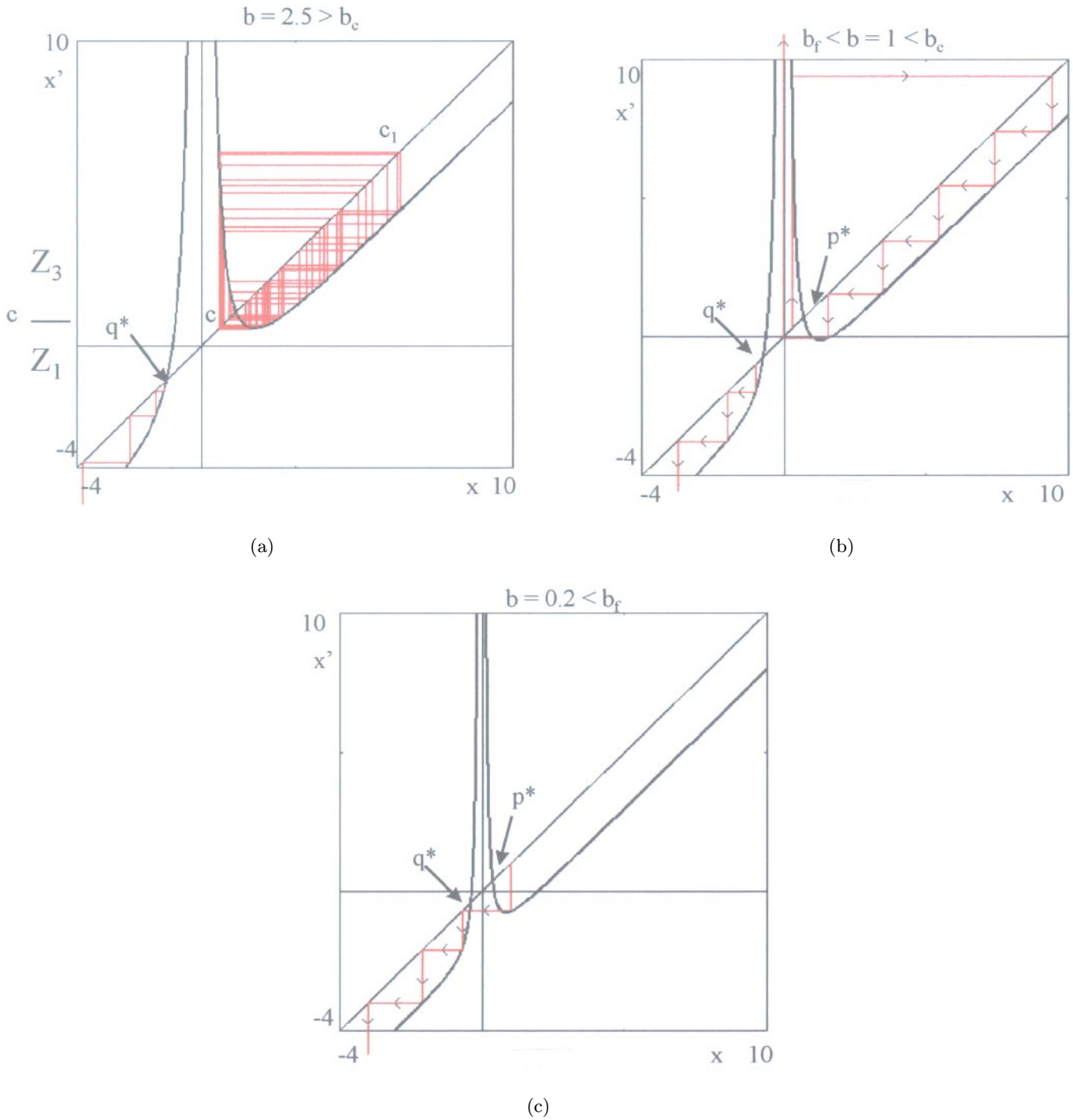
Fig. 5.   Graph of the map (19) for three different values of the parameter b. (a) $b > b_c$: Two trajectories are represented, one starting with $x_0 < q^*$, which diverges to $-\infty$, one starting with $x_0 > q^*$ which enters the bounded absorbing interval $[c, c_1]$. (b) $b_f < b < b_c$: Two trajectories are represented, one starting with $x_0 < q^*$, which diverges to $-\infty$, one starting with $x_0 > q^*$ which is not divergent, but involves arbitrarily large values of x. (c) $b < b_f$: the generic trajectory diverges to $-\infty$.

has two repelling fixed points, $z = 0$ and $z = 1$, corresponding, respectively, to $x = -\infty$ and $x = +\infty$ by the homeomorphism (18).

To sum up, *the chaotic trajectories generated by the map (16) include arbitrarily large values, due to the presence of the vertical asymptote, but such trajectories do not diverge, because the infinity is repelling.* This is the basic mechanism for the existence of an unbounded chaotic set.

3.2. *Contact bifurcations causing the appearance and the disappearance of unbounded nondiverging trajectories*

Let us consider the one-dimensional noninvertible map

$$x' = f_b(x) = x + \frac{b}{x^2} - 2, \quad b > 0 \qquad (19)$$

whose set of nondefinition, due to the vanishing of the denominator, is $\delta_s = \{0\}$. The graph of (19) is characterized by the presence of a vertical asymptote at $x = 0$ and an oblique asymptote of equation $x' = x - 2$. The map (19) is noninvertible following the terminology of [Mira *et al.*, 1996a], it is a $Z_1 - Z_3$ map, because the critical point

$$c = \sqrt[3]{2b} + \sqrt[3]{\frac{b}{4}} - 2, \qquad (20)$$

image of $c_{-1} = (2b)^{1/3}$, local minimum of $f_b(x)$, separates the range of the map into the intervals $Z_1 = (-\infty, c)$ and $Z_3 = (c, +\infty)$ whose points have one or three preimages respectively [see Fig. 5(a)]. The critical point c is characterized by two merging preimages, located in $c_{-1} = \sqrt[3]{2b}$. The map (19) has two fixed points at finite distance:

$$q^* = -\sqrt{\frac{b}{2}} \quad \text{and} \quad p^* = \sqrt{\frac{b}{2}} \qquad (21)$$

It is immediate to see that q^* is repelling for any $b > 0$, whereas p^* is stable for $b > 8$, and at $b = 8$ it loses stability via a flip bifurcation, which creates a stable cycle of period 2, followed, as b is further decreased, by a sequence of period-doubling bifurcations, leading to the creation of chaotic attractors, and by the complex sequence of bifurcations known as "box-within-a-box" structure, typical of unimodal maps (see e.g. [Mira, 1987]).

As far as $c > 0$, any trajectory $\{x_n = f_b^n(x_0)\}$ with $x_0 > q^*$ enters the interval $I = [c, c_1]$, with $c_1 = f_b(c)$, and then never escapes, i.e. such trajectories are ultimately bounded inside I. The interval I is called absorbing interval (see [Mira *et al.*, 1996]), and inside I the asymptotic dynamics may converge to the fixed point p^* (for $b > 8$) or to an attracting cycle or to a bounded chaotic attractor.

The unstable fixed point q^* constitutes the boundary which separates the basin of attraction $\mathcal{B}(I) = (q^*, +\infty)$ of the absorbing interval I, defined as the set of points whose trajectories have ω-limit sets inside I, from the basin of infinity $\mathcal{B}(-\infty) = (-\infty, q^*)$, defined as the set of points which generate trajectories diverging to $-\infty$. We can say that for the map (19) $-\infty$ is attracting and $+\infty$ is repelling. This means that points arbitrarily close to $+\infty$ are mapped into points of smaller modulus until they enter I after a finite number of iterations, whereas points sufficiently close to $-\infty$ generate sequences diverging to $-\infty$. In Fig. 5(a), obtained for $b = 2.5$, two trajectories are represented by the König–Lemeray staircase diagram: one, starting from $x > q^*$, shows an apparently chaotic behavior inside I, the other one is a diverging trajectory starting from $x = -1.2 < q^*$.

As b decreases, the critical point c also decreases, until it reaches the value $c = 0$ at $b = b_c = 32/27$. This contact between the critical point c and the point $x = 0$, belonging to δ_s, marks the occurrence of a bifurcation at which the bounded absorbing interval I is transformed into an interval which is not bounded above. In fact, $c_1 \to +\infty$ as $b \to b_c^+$, and for $b < b_c$ we have $c < 0$. This implies that after the contact bifurcation the trajectories starting with $x_0 > q^*$ may involve arbitrarily large values, even if they are not divergent. In Fig. 5(b) the early points of a typical trajectory obtained with $b < b_c$, and starting from $x_0 = 0.3 > q^*$, are shown. In the same figure also a typical diverging trajectory starting from $x = -1 < q^*$ is represented, so that the difference between a diverging trajectory and an unbounded not diverging trajectory can be easily seen.

The bifurcations described above can also be seen by a bifurcation diagram, like the one shown in Fig. 6(a). This bifurcation diagram is obtained by the usual procedure: For each value of the parameter b a trajectory starting from the critical point is numerically generated and, after a transient of the early 1000 iterates has been discarded, 3000 points are plotted along the vertical line through b. For $b > 8$ the asymptotic dynamics is characterized by convergence to a fixed point [this is not visible in the range of b considered in Fig. 6(a)], then for decreasing values of b the usual sequence of period-doubling bifurcations leading to chaotic behavior, and the "box-within-a box" bifurcation structure typical of unimodal maps, is obtained. At $b = b_c$, the contact bifurcation, at which the absorbing interval $[c, c_1]$ becomes unbounded, is revealed by a sudden decrease of the density of the iterated points, due to the fact that they are distributed over an unbounded interval. Just after the

100

x

c_1

- 2

0.3 b_f $b_c \cong 1.185$ c b 5

(a)

4

x

- 1

0.58 b 0.7
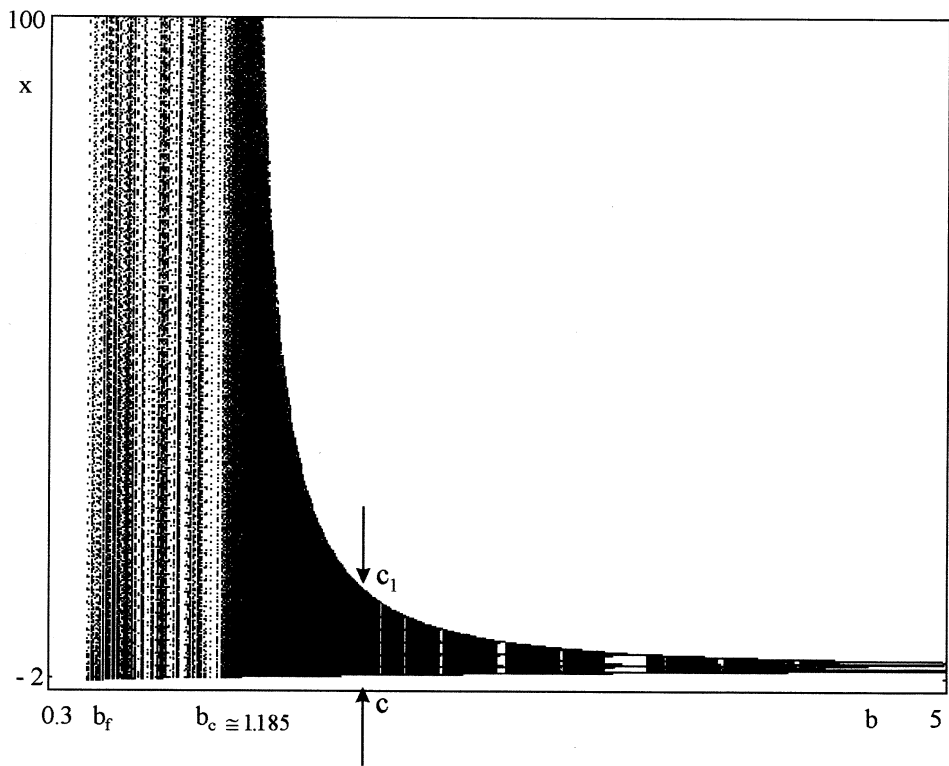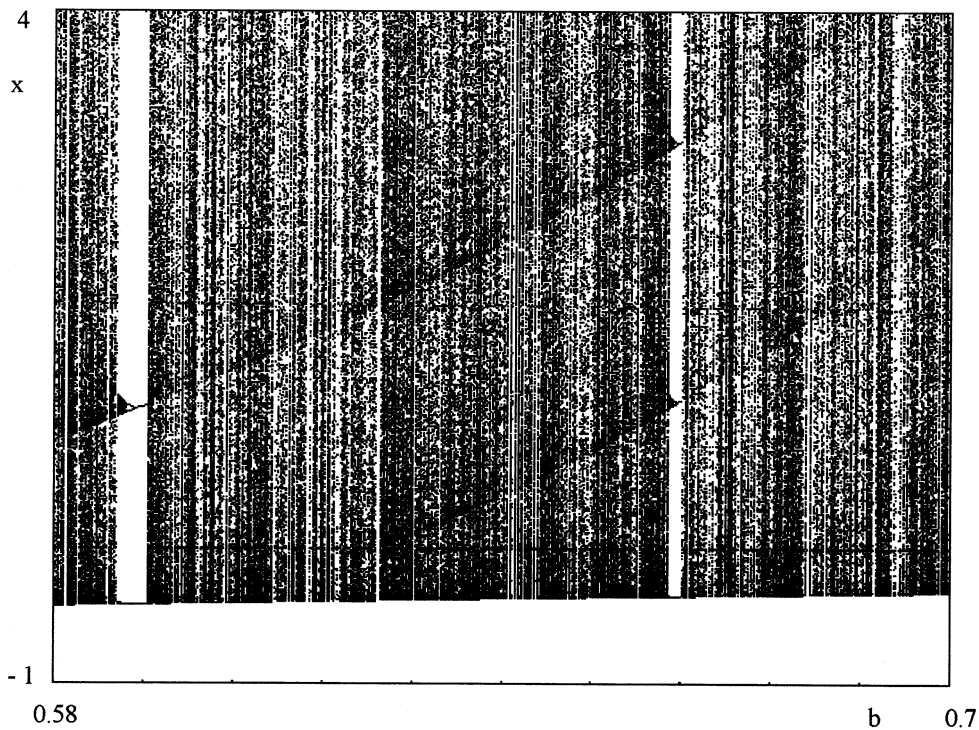
(b)

Fig. 6.   (a) Bifurcation diagram for the map (19). For each value of b, 4000 points of the trajectory starting from the critical point are numerically generated, and the last 3000 are plotted along the vertical line $x = b$. For $b > b_c$ the asymptotic values are trapped inside the bounded absorbing interval $[c, c_1]$. For $b < b_c$ they are spread along an interval without any upper bound. (b) Enlargement of a portion of the bifurcation diagram shown in (a): two windows (or boxes) associated with stable periodic orbits, of periods two and three respectively, are clearly visible. It is easy to prove that infinitely many such boxes exist for $b_f < b < b_c$, associated with stable cycles of any order, in a complex sequence of "box-within-a-box" bifurcation structure.

1446

(a)

(b)
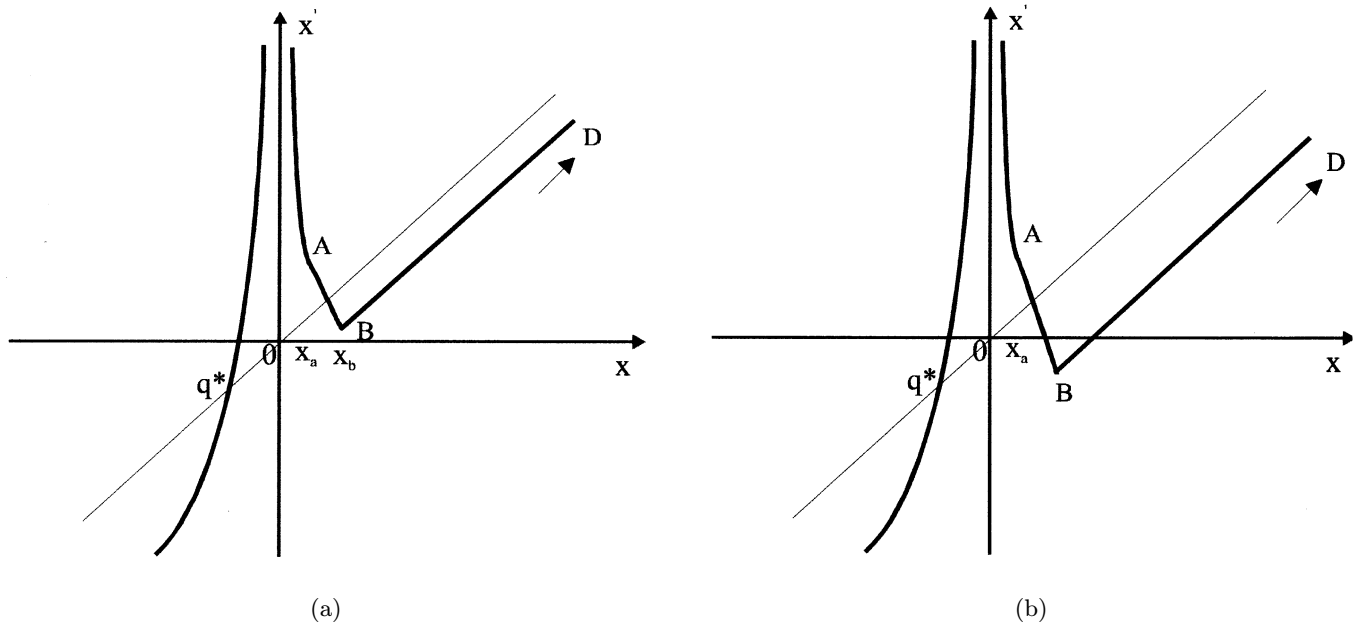
Fig. 7. A piecewise smooth version of the map (19). For $x < 0$ the slope is always greater than 1, for $0 < x < x_a$ and $x_a < x < x_b$ the slopes are less than -1, for $x > x_b$ the slope is equal to 1. (a) If the relative minimum B is above the x axis then the generic initial condition $x_0 > q^*$ generates a chaotic trajectory, ultimately bounded inside the interval $[B, f(B)]$. (b) If the relative minimum B is below x and above the unstable fixed point q^* then the generic initial condition $x_0 > q^*$ generates an unbounded chaotic trajectory which densely covers the interval $[B, +\infty)$.

bifurcation, for $b < b_c$, other sequences of "box-within-a-box" bifurcations occur. The "windows" associated with attracting cycles of periods two and three, obtained for values of the parameters b approximately given by $b = 0.5921$ and $b = 0.66389$ respectively, are clearly visible in the enlargement of a portion of the bifurcation diagram, with $b < b_c$, shown in Fig. 6(b).

For $b < b_c$, even if a bounded attractor exists, generally an attracting cycle of very high period, the trajectories converging to it may have an unbounded transient, i.e. a transient involving arbitrarily large values of x_n. Moreover, no upper bound exists for the periodic points.

It is easy to modify the shape of the function in order to get a map for which we have "persistent" unbounded chaotic attractors. Consider the graph of the map shown in Fig. 7(a). The unbounded branch on the left, for $x < 0$, may be assumed like that of the map (19), with slope always greater than 1. For $x > 0$ the map of Fig. 7 is piecewise smooth, made up of three portions which have slopes less than -1 for $0 < x < x_a$ and for $x_a < x < x_b$, and slope equal to 1 for $x > x_b$ (the two portions with $x_a < x < x_b$ and $x > x_b$ may be considered linear). Now assume that a parameter, say b, decreases, the minimum B moves downwards until it crosses the x

axis at $b = b_c$, it becomes negative [like in Fig. 7(b)] and then it assumes the same ordinate as the unstable fixed point q^* at $b = b_f$. This implies that as far as b is in the interval $(b_f, b_c]$ no attracting cycles can exist, and the dynamics are chaotic in the whole unbounded absorbing interval $I = [B, +\infty)$.

Now consider again the map (19). It can be noticed that for $b > b_c$, i.e. before the contact, any trajectory starting with $x_0 > 0$ is trapped in the region $x > 0$, and any trajectory starting with $x_0 \in (q^*, 0)$ is mapped into the region $x > 0$ after a finite number of iterations. This implies that for $b > b_c$ the asymptotic dynamics of nondiverging trajectories is ultimately bounded into the absorbing interval $I = [c, c_1]$, and it is only determined by the branch of the graph of f_b with $x > 0$, so that the asymptotic dynamics are essentially that of a unimodal map. Instead, after the contact, i.e. for $b < b_c$, the region $x > 0$ is no longer trapping, since the points in a neighborhood of the minimum c_{-1} are mapped in the region $x < 0$, so that the asymptotic dynamics also involve the left branch of the graph. This implies that the asymptotic behavior is no longer that of a unimodal map: loosely speaking, we can say that the map behaves like a bimodal map, with a maximum at $c_{-1}^M = 0$, even if the corresponding critical point c^M is at $+\infty$.
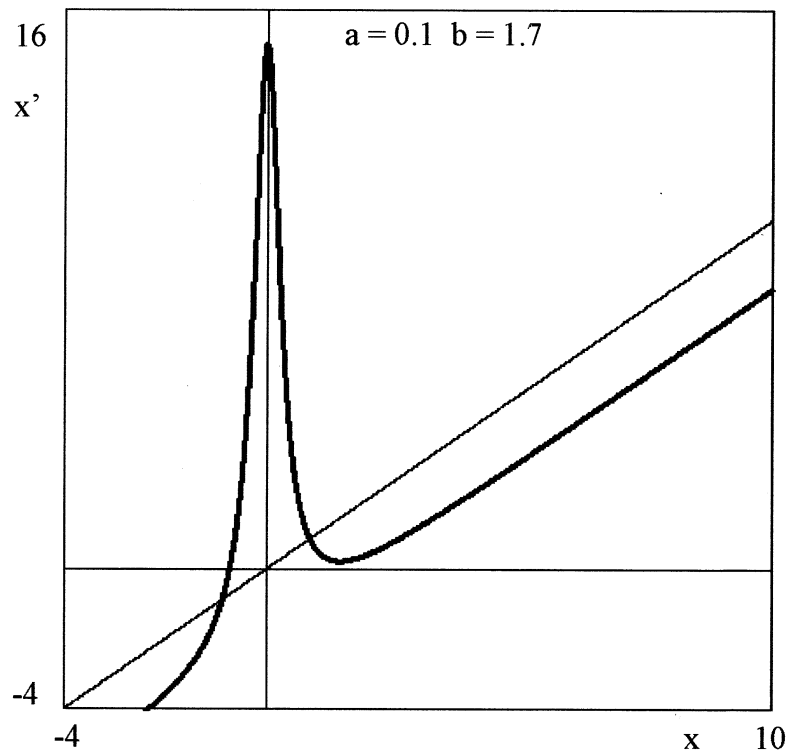
(a)
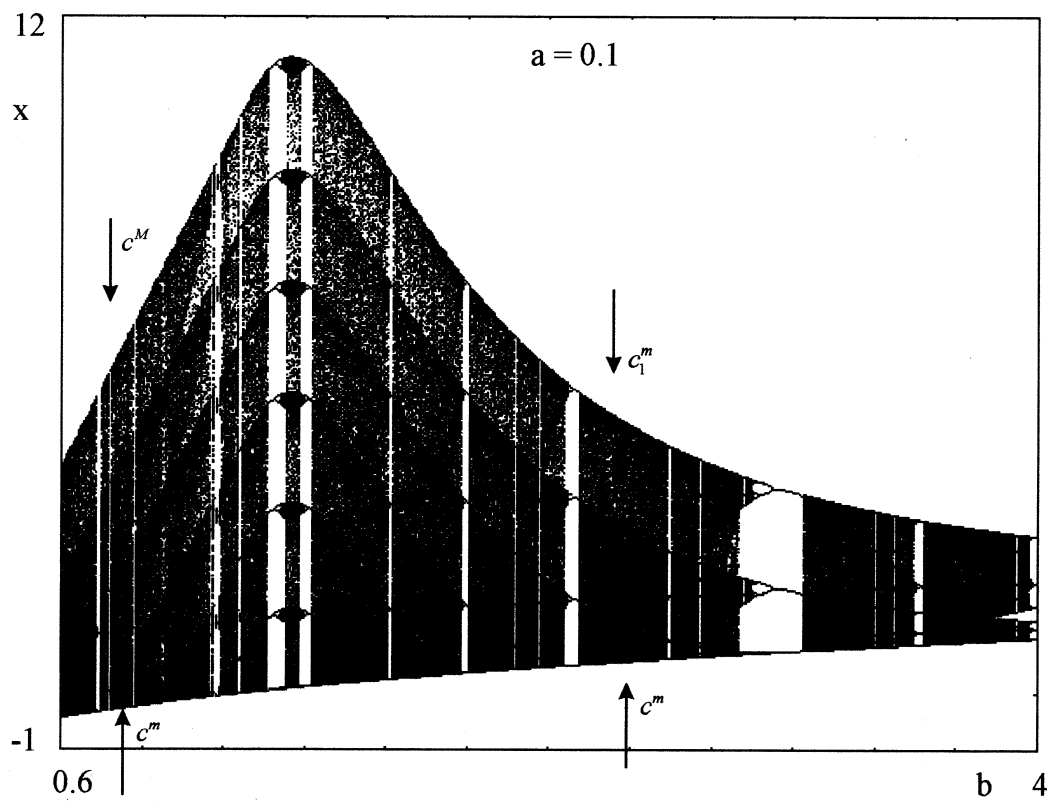
(b)

Fig. 8.   (a) Graph of the map (22) with parameters $a = 0.1$ and $b = 1.7$.   (b) Bifurcation diagram which represents the asymptotic behavior of the map (22) with $a = 0.1$ and $b \in [0.6, 4]$.

To emphasize more this point, we may consider the map (19) as a limiting case of a bimodal map, such as

$$x' = f_{a,b}(x) = x + \frac{b}{x^2 + a} - 2, \quad a > 0, \; b > 0. \quad (22)$$

This map has a local minimum, say c^m_{-1}, with critical point $c^m = f_{a,b}(c^m_{-1})$ which decreases as b decreases, and a local maximum c^M_{-1}, such that $c^M_{-1} \to 0^+$ as $a \to 0^+$, with critical point $c^M = f_{a,b}(c^M_{-1})$ such that $c^M \to +\infty$ as $a \to 0^+$ [the graph of the map (22) is shown in Fig. 8(a)]. Also the asymptotic dynamics of the map (22) shows a change as b decreases, due to the merging of c^m and c^M_{-1} (which implies $c^m_1 = c^M$). Before this merging, the nondiverging trajectories are ultimately bounded inside the absorbing interval $I = [c^m, c^m_1]$, where the dynamic behavior is that of a unimodal map, whereas when $c^m < c^M_{-1}$ the nondiverging trajectories are ultimately bounded inside the absorbing interval $J = [c^m, c^M]$, where the dynamic behavior is that of a bimodal map since the absorbing interval includes both the local extrema. This can be seen in the bifurcation diagram of Fig. 8(b), where the asymptotic behavior of the map (22) is represented as a function of the parameter b with the parameter a fixed at the value $a = 0.1$. The condition $c^m_1 = c^M$ corresponds with the maximum amplitude of the absorbing interval inside which the asymptotic dynamics are ultimately trapped, because c^m_1 decreases with b, whereas c^M is an increasing function of b. In the limiting case $a \to 0^+$ the behavior of the recurrence remains essentially the same for $b > b_c$, bounded inside $I = [c^m, c^m_1]$, because the vanishing of the parameter a does not have a big effect on the critical point c^m. Instead, for $b < b_c$ the absorbing interval J becomes unbounded, since it includes the singular point $x = 0 \in \delta_s$.

We now consider, again, the map (19). For $b < b_c$, just after the contact bifurcation at which the absorbing interval is transformed from a bounded interval $I = [c, c_1]$ into an unbounded interval $I = [c, +\infty)$, the basin of I is still $\mathcal{B}(I) = (q^*, +\infty)$, and also the basin of infinity is unchanged, given by $\mathcal{B}(-\infty) = (-\infty, q^*)$. Another important bifurcation occurs at $b = b_f = 1/2$, when the critical point c has a contact with the basin boundary, i.e. $c = q^*$. This is the *final bifurcation* (or *boundary crisis*) which causes the disappearance of the unbounded absorbing interval. For $b < b_f$ the generic trajectory diverges to $-\infty$ [see Fig. 5(c)].

3.3. *A chaotic recurrence with analytic closed form solution*

Another example of a one-dimensional recurrence characterized by chaotic and unbounded trajectories is obtained by the iteration of the map

$$x' = f(x) = \frac{x^2 + 2x - 1}{2x^2}. \quad (23)$$

This map is not defined for $x = 0$, where the graph has a vertical asymptote (see Fig. 9) and the recurrence $x_{n+1} = f(x_n)$ is well defined if the restriction of f to the set $E = \mathbb{R} \setminus \bigcup_{k \geq 0} f^{-k}(0)$ is considered. The map (23) has three fixed points:

$$x^*_1 = -1, \; x^*_2 = \frac{1}{2}, \; x^*_3 = 1$$

with multipliers

$$f'(x^*_1) = -2, \; f'(x^*_2) = 4, \; f'(x^*_3) = 0$$

respectively. From the graph shown in Fig. 9 it is evident that the fixed point x^*_2 constitutes the boundary which separates the basin of the stable fixed point x^*_3, given by $\mathcal{B}(x^*_3) = E \cap (1/2, +\infty)$, from the subset of E with $x < 1/2$, whose points generate complex trajectories which appear to move erratically in the whole interval $(-\infty, 1/2)$.

Indeed, the trajectories starting with an initial condition $x_0 < 1/2$ are unbounded and chaotic. In fact, a peculiarity of the map (23) is that for the recurrence

$$x_{n+1} = f(x_n), \quad x_0 \in E \quad (24)$$

it is possible to write the general solution x_n, $n \geq 0$, in closed form and in terms of elementary algebraic and transcendental functions.

If $x_0 \leq 1/2$ then the solution is

$$x_n = \frac{\cos(2^n C)}{1 + \cos(2^n C)}, \quad \text{with} \quad C = \arccos \frac{x_0}{1 - x_0} \quad (25)$$

where the arccos function is, as usual, the inverse of the cosine function that maps the interval $[-1, 1]$ to the interval $[0, \pi]$.

If $x_0 \in (1/2, 1)$ then the solution is

$$x_n = \frac{\cosh(2^n K)}{1 + \cosh(2^n K)}, \quad \text{with} \quad K = \cosh^{-1} \frac{x_0}{1 - x_0} \quad (26)$$
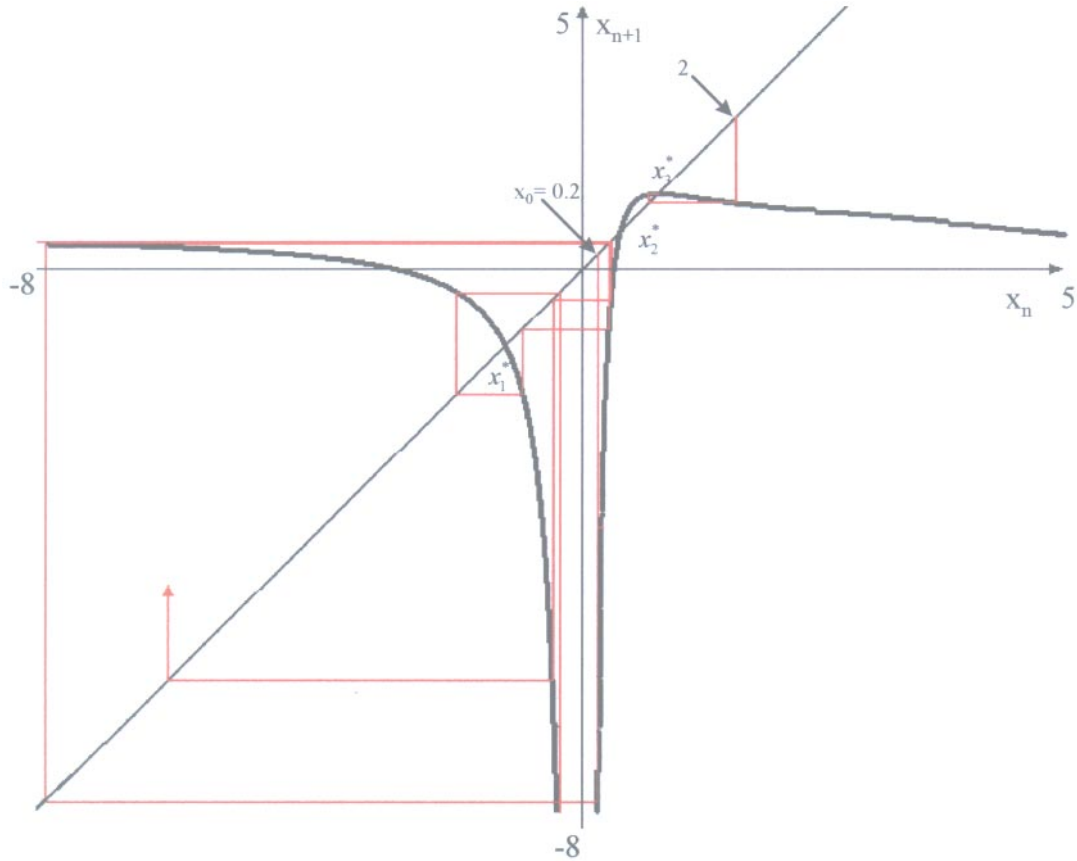
Fig. 9.   Graph of the map (23) together with the König–Lemeray staircase diagram of two typical trajectories: an unbounded chaotic trajectory, starting with $x_0 = 0.2$, whose points can be analytically computed by (25) x; a trajectory starting with $x_0 = 2$ and converging to x_3^*.

where the $\cosh^{-1}$ function is the inverse of the hyperbolic cosine function that maps the interval $[1, +\infty)$ to $[0, +\infty)$. Furthermore, if $x_0 > 1$ then its image $x_1 \in (1/2, 1)$, hence (26) holds with n shifted by 1.

These solutions can be easily checked by direct substitution inside the recurrence (24). For

example, for the solution (25) we have

$$x_{n+1} = \frac{\cos 2(2^n C)}{1 + \cos 2(2^n C)} = \frac{2\cos^2(2^n C) - 1}{2\cos^2(2^n C)}$$

where the duplication formula of cosine has been used, and

$$f(x_n) = \frac{\cos^2(2^n C) + 2\cos(2^n C)(1 + \cos(2^n C)) - [1 + \cos(2^n C)]^2}{2\cos^2(2^n C)} = \frac{2\cos^2(2^n C) - 1}{2\cos^2(2^n C)}.$$

The solution (26) can be analogously verified.

The possibility to explicitly write the closed form solution for the recurrence (24) is due to the fact that the map (23) has been obtained by a particular procedure, based on the Schröder functional equation, as shown in the Appendix A.

From (26) it is easy to see that every trajectory starting from an initial condition $x_0 \in (1/2, 1)$

is an increasing sequence converging to $x_3^* = 1$. From the arguments given above, the convergence to x_3^* also holds for all the trajectories starting with $x_0 > 1$.

For the purposes of this paper the most interesting trajectories are those generated starting with $x_0 < 1/2$, since any trajectory whose points are obtained by (25) is chaotic and its points are

spread along the whole unbounded chaotic interval $(-\infty, 1/2)$. In fact, every sequence expressed by $P(2^n C)$, where P is a periodic function, exhibits sensitive dependence on initial conditions [Mira, 1987; Mira *et al.*, 1996]) and is a candidate to be conjugate to the shift-map [Brown & Chua, 1996].

We observe that, like in the two examples examined in the previous subsections, *a point of nondefinition, given by $x = 0$ in this case, is included in the closure of the unbounded chaotic set*, given by $E \cap (-\infty, 1/2)$ in this case. As argued in Sec. 2, this is a necessary condition to have an unbounded set of attraction in an iterated map with a denominator which can vanish.

In this example the point $x = 0$ plays the role of a "minimum" (critical point c_{-1} of rank-0) of $f(x)$, with related "minimum value" (critical point c of rank-1) at $-\infty$. In the same limiting sense, the critical point $c = -\infty$ may be thought to be mapped in $c_1 = f(c) = x_2^*$. So, the chaotic interval $(c, c_1) = (-\infty, x_2^*)$ totally fills up its basin. It is worth noticing that the maps generated by the method based on the Schröder equation (described in the Appendix A) have the above property, i.e. in general they lead to chaotic solutions which totally fill up their immediate basin, as indicated in [Mira, 1987] and [Mira *et al.*, 1996a]. We also remark that the method used to obtain the chaotic map (23), based on the Schröder functional equation, is a general and easy method to obtain maps with chaotic trajectories which can be written in a closed form. By a proper choice of the functions (like the one called g in the Appendix A) many recurrences with a vanishing denominator, characterized by the presence of unbounded chaotic trajectories, can be easily obtained. This method can be extended to two-dimensional maps, as we shall see in the first example of the next section.

4. Two-Dimensional Examples

Unbounded sets of attraction are easily observed in two-dimensional recurrences obtained by the iteration of a map $T : (x, y) \rightarrow (x', y')$ which is not defined in the whole plane, due to the presence of one or more curves at which a denominator vanishes. For noninvertible two-dimensional maps, unbounded sets of attraction may be created by contact bifurcations similar to the one described in Sec. 3.2. In fact, a curve which belongs to the set of nondefinition δ_s may be considered as a two-dimensional analogue of a vertical asymptote. As

argued in Sec. 2, if A is an attracting set for the recurrence $(x_{n+1}, y_{n+1}) = T(x_n, y_n)$, and some portion of δ_s is included inside the closure of A, then A may be an unbounded set of attraction. Moreover, for a two-dimensional noninvertible map, a chaotic area A is often bounded by segments of critical curves $LC_i = T^i(LC)$, where LC is the critical curve of rank-1 (the two-dimensional analogue of critical points of one-dimensional maps, see e.g. [Gumowski & Mira, 1980; Mira *et al.*, 1996; Abraham *et al.*, 1997]. Hence, the first crossing of A with δ_s occurs just after the first contact between a critical curve, on the boundary of A, and δ_s. This represents the two-dimensional analogue of the contact bifurcation occurring at $b = b_c$ for the one-dimensional map (19).

4.1. *From bounded to unbounded chaotic sets in a two-dimensional recurrence*

Let us consider the two-dimensional recurrence $(x_{n+1}, y_{n+1}) = T(x_n, y_n)$ where T is defined by

$$T : \begin{cases} x' = \dfrac{y^2 + 2xy - x^2 - 2x - 2y + b}{x^2 + 6xy + y^2 - 6x - 6y + 3} \\[2mm] y' = \dfrac{x^2 + 2xy - y^2 - 2x - 2y + b}{x^2 + 6xy + y^2 - 6x - 6y + 3} \end{cases} \quad (27)$$

The set δ_s is given by

$$\delta_s = \{(x, y) \in \mathbb{R}^2 | x^2 + 6xy + y^2 - 6x - 6y + 3 = 0\}$$

which is an hyperbola with centre in $(3/4, 3/4)$ and symmetry lines of equation $y = x$ and $y = -x + 3/2$. The recurrence obtained by the iteration of the map (27) is well defined provided that the initial condition $(x_0, y_0) \in E$, where E is the trapping set defined in (7).

The map (27) is symmetric with respect to the reflection through the diagonal $\Delta = \{(x, x) \in \mathbb{R}^2\}$. In fact, if we denote by $S : (x, y) \rightarrow (y, x)$ the map which reflects through Δ, we have that T commutes with S, i.e. $S(T(x, y)) = T(S(x, y))$. This symmetry property implies that any orbit $G = \{(x_n, y_n)\}$ of T is either symmetric with respect to Δ, i.e. for each point $(x_n, y_n) \in G$ also $S(x_n, y_n) \in G$, or the set $S(G) = \{S(x_n, y_n)\}$, symmetric of G with respect to Δ, is an orbit of T as well. This also implies that $T(\Delta) \subseteq \Delta$, i.e. $x = y$ implies $x' = y'$. Hence the diagonal Δ is a trapping one-dimensional submanifold for T, and the trajectories embedded inside Δ are governed by the restriction of T to Δ,
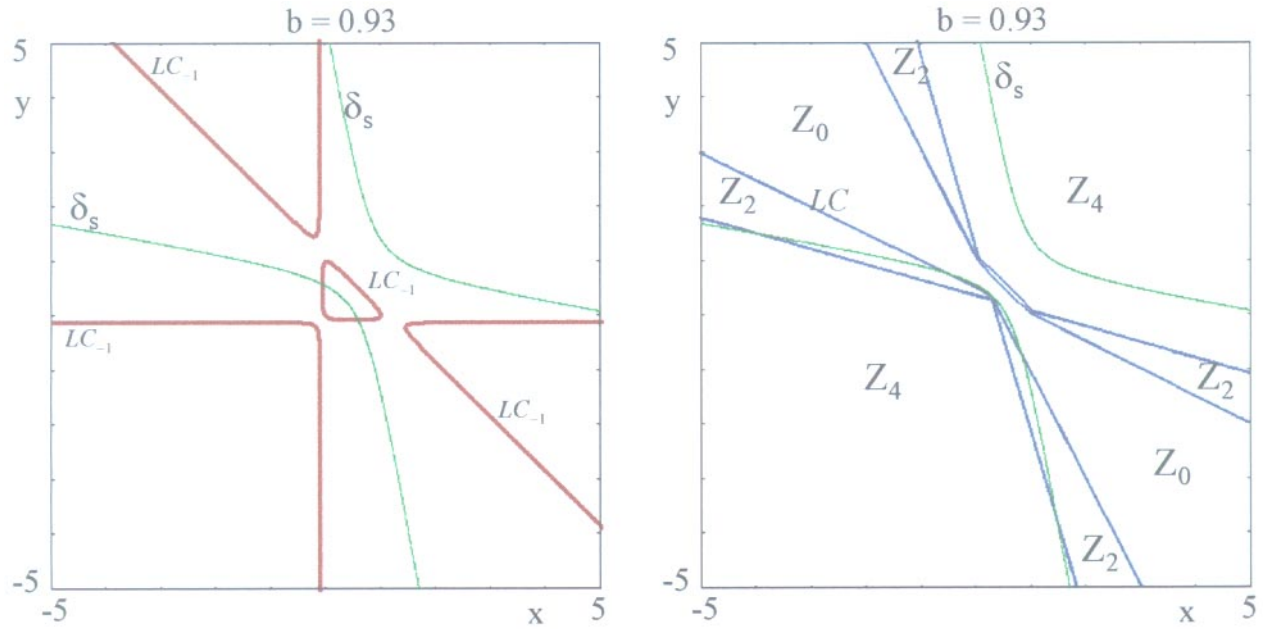
(a)
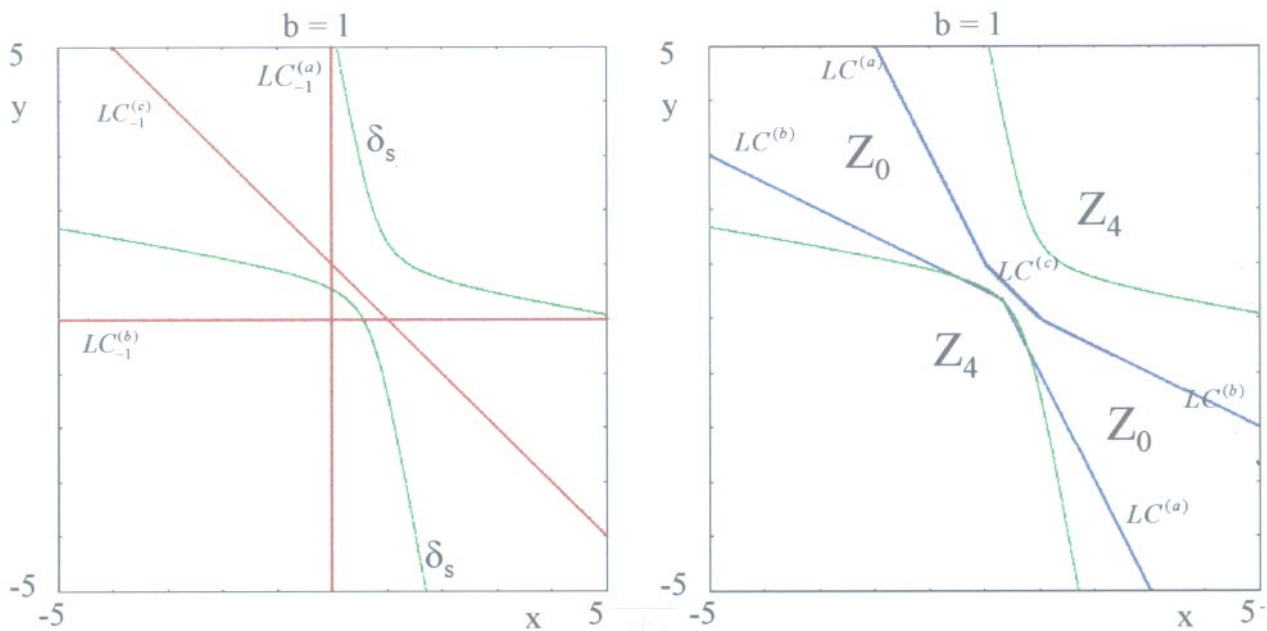
(b)

Fig. 10.   (a) Critical set of rank-0, LC_{-1}, (on the left) and critical set of rank-1, LC, (on the right) for the map (27) with $b = 0.93$. (b) Critical set of rank-0, LC_{-1}, (on the left) and critical set of rank-1, LC, (on the right) for the map (27) with $b = 1$. In all the figures the set of nondefinition δ_s, given by the hyperbola of Eq. (29), is represented by the green curve.

$T|_\Delta : \Delta \to \Delta$, which can be identified with the one-dimensional map

$$z' = g(z) = \frac{2z^2 - 4z + b}{8z^2 - 12z + 3} \qquad (28)$$

obtained by setting $x = y = z$ and $x' = y' = z'$ in (27).

   The map (27) is a noninvertible map of $Z_0 - Z_2 - Z_4$ type, where Z_0, Z_2 and Z_4 represent the regions of the phase plane whose points have two or

four distinct rank-1 preimages respectively. These regions are separated by the *critical set of rank-1 LC*, defined as the locus of points having at least two merging preimages, located on the so-called *critical set of rank-0*, denoted by LC_{-1} (we follow the notations of [Mira *et al.*, 1996]). The set LC_{-1} is obtained as the locus of points where the Jacobian determinant of T, $\det DT(x, y)$, vanishes, and $LC = T(LC_{-1})$ (see [Mira *et al.*, 1996] for more complete definitions). For the map (27) the condition $\det DT(x, y) = 0$ becomes

$$b(3x^2 + 3y^2 + 2xy - 3x - 3y)$$
$$- 3x^2 - 3y^2 - 2x^2y - 2xy^2 + 3x + 3y = 0. \quad (29)$$

The set of points which satisfy (29), i.e. the set LC_{-1} of the map (27), is represented by the red curves of Fig. 10(a), obtained with $b = 0.93$, and its image $LC = T(LC_{-1})$ is represented by the blue curves, which separate the regions Z_i characterized by different number of preimages. In Fig. 10 also the set of nondefinition δ_s is represented.

A particular case is obtained for $b = 1$, as in this case Eq. (29) reduces to $2xy(1 - x - y) = 0$, so that LC_{-1} is given by the union of three lines

$$LC_{-1} = LC_{-1}^{(a)} \cup LC_{-1}^{(b)} \cup LC_{-1}^{(c)}$$
$$= \{x = 0\} \cup \{y = 0\} \cup \{y = 1 - x\} \quad (30)$$
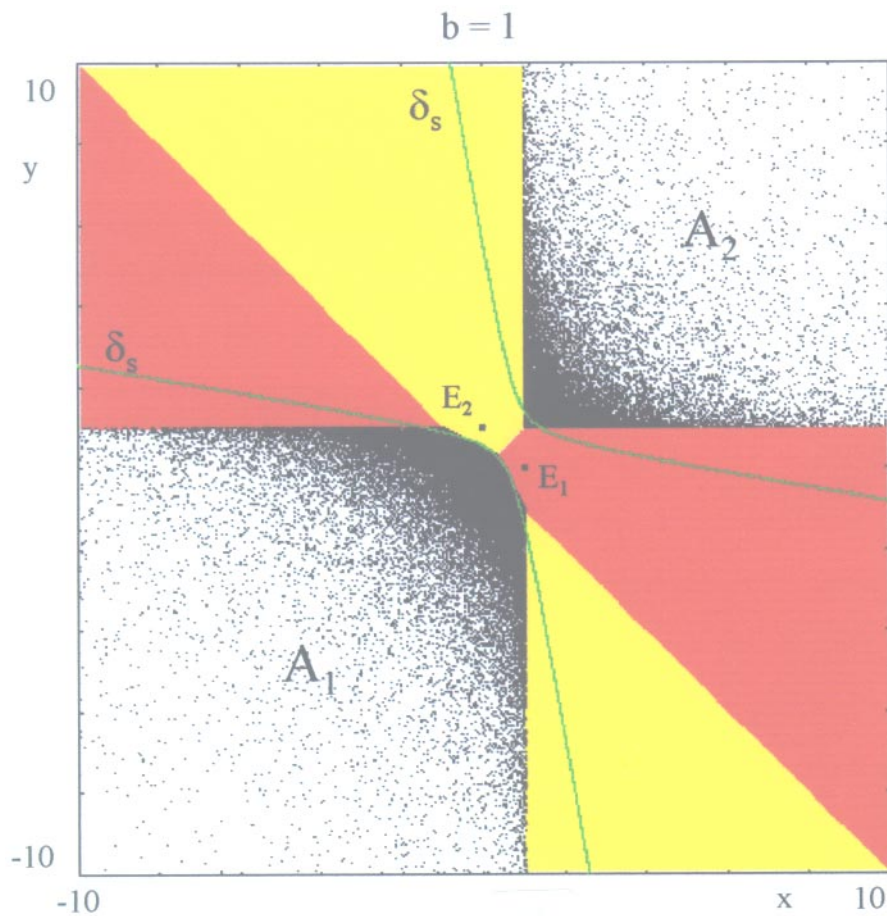
(a)

Fig. 11. (a) The numerically generated points of a typical chaotic trajectory of the map (27) with $b = 1$ are represented by black dots, which cover the unbounded chaotic area $A(1) = A_1 \cup A_2$ defined in (31). The red and yellow regions represent the basins of the stable fixed points E_1 and E_2 respectively. (b) Two images of the portion of LC_{-1} included inside the chaotic area $A(1)$, belonging to the critical curves $LC = T(LC_{-1})$ and $LC_1 = T(LC)$ respectively, are enough to cover the whole boundary of the chaotic area $A(1)$. In both figures, the set of nondefinition δ_s, given by the hyperbola of Eq. (29), is represented by the green curve.
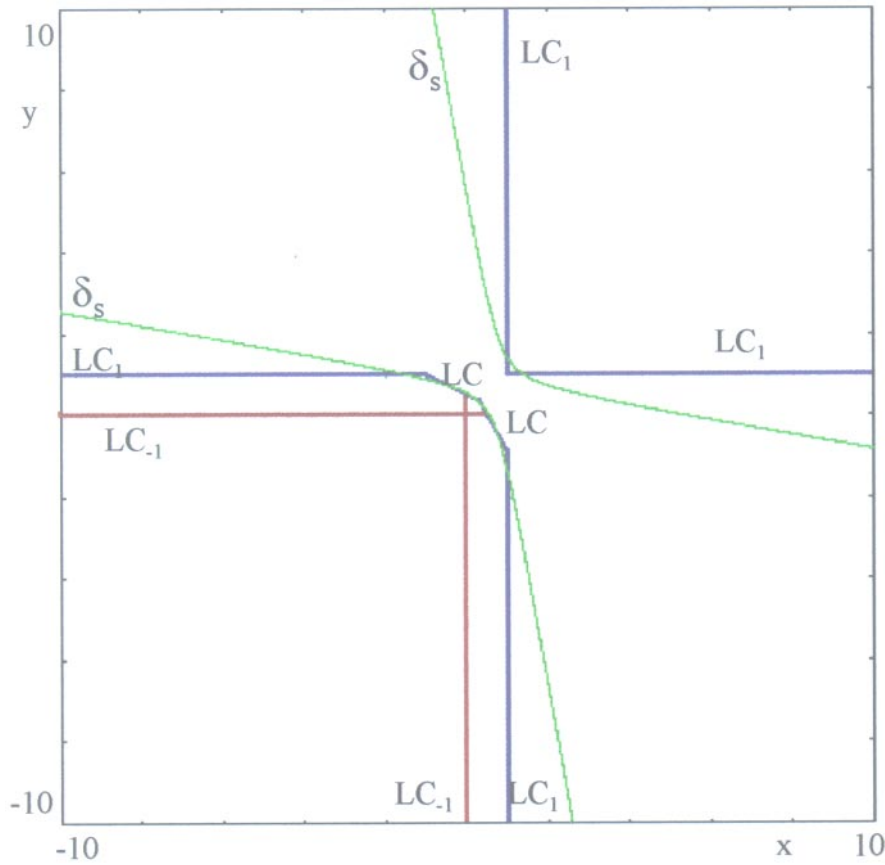
(b)

Fig. 11.   (Continued)

represented by the red curves of Fig. 10(b). In this particular case, also the equations of the curves which form the critical set

$$LC = LC^{(a)} \cup LC^{(b)} \cup LC^{(c)}$$

$$= T(LC_{-1}^{(a)}) \cup T(LC_{-1}^{(b)}) \cup T(LC_{-1}^{(c)})$$

can be analytically computed:

$$LC = T\{x = 0\} \cup T\{y = 0\} \cup T\{x + y = 1\}$$

$$= \{2x + y = 1\} \cup \{x + 2y = 1\} \cup \{x + y = 1\}$$

as shown by the blue curves of Fig. 10(b).

The map (27) with $b = 1$ has the peculiar property that for any initial condition $(x_0, y_0) \in A(1)$, where $A(1) = A_1 \cup A_2$ with

$$A_1 = \{(x, y) \in \mathbb{R}^2 | x < 1 \text{ and}$$

$$y < 1 \text{ and } 2x + y < 1 \text{ and } x + 2y < 1\}$$

$$A_2 = \{(x, y) \in \mathbb{R}^2 | x > 1 \text{ and } y > 1\} \qquad (31)$$

the recurrence $(x_{n+1}, y_{n+1}) = T(x_n, y_n)$, obtained by the iteration of T, has a closed form solution $\{x_n, y_n\}$ expressed in terms of elementary functions

$$x_n = \frac{\cos(2^n C_1)}{\cos(2^n C_1) + \cos(2^n C_2)},$$

$$y_n = \frac{\cos(2^n C_2)}{\cos(2^n C_1) + \cos(2^n C_2)} \qquad (32)$$

where the constants C_1 and C_2 are determined by the initial condition $(x_0, y_0) \in A$

$$C_1 = \arccos \frac{x_0}{x_0 + y_0 - 1}, \quad C_2 = \arccos \frac{y_0}{x_0 + y_0 - 1}.$$

Indeed, the map (27) with $b = 1$ has been obtained by the method described in the Appendix B, based on the Schröder functional equation (see [Gumowski & Mira, 1980; Mira et al., 1996, Chap. 1]). The sequence (32) defines a typical chaotic trajectory, characterized by sensitive dependence on initial conditions, which spans the whole
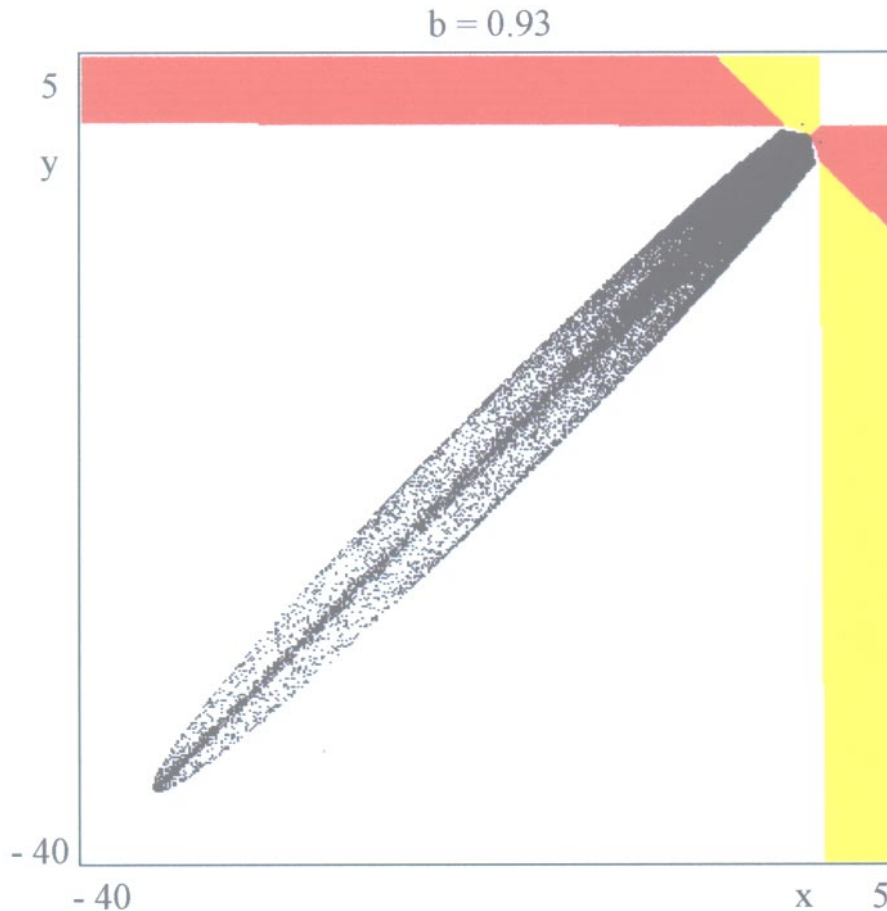
Fig. 12. A trajectory of the map (27) with $b = 0.93$ which belongs to an absorbing area bounded by critical curves.

chaotic area $A(1)$. Hence $A(1)$ is an unbounded chaotic area. In Fig. 11(a) the early points of a trajectory starting inside $A(1) = A_1 \cup A_2$ are represented, and in Fig. 11(b) we show that the boundary of the chaotic area $A(1)$ can be obtained by segments of critical curves. Indeed, the images of the portions of LC_{-1} which are included inside $A(1)$ are sufficient to bound the chaotic area (see [Mira *et al.*, 1996, Chap. 4]). This implies that $LC_{-1}^{(c)}$ can be neglected in order to obtain such a boundary. Moreover, two images of the portions of $LC_{-1}^{(a)}$ and $LC_{-1}^{(b)}$, given by

$$LC^{(a)} \cup LC^{(b)} = T(\{x = 0\}) \cup T(\{y = 0\})$$

$$= \{2x + y = 1\} \cup \{x + 2y = 1\}$$

and

$$LC_1^{(a)} \cup LC_1^{(b)} = T(\{2x + y = 1\}) \cup T(\{x + 2y = 1\})$$

$$= \{x = 1\} \cup \{y = 1\}$$

are sufficient to obtain the complete boundary of $A(1)$ [see Fig. 11(b)].

In the case $b = 1$, the initial conditions belonging to the set complementary to $A(1)$, i.e. $(x_0, y_0) \in E \setminus A(1)$, generate trajectories converging to one of the stable fixed points $E_1 = (1, 0)$ and $E_2 = (0, 1)$, whose basins are represented in Fig. 11(a) by the red and yellow regions respectively. In the particular case $b = 1$, also, the lines $x = 1$ and $y = 1$ are trapping lines, and belong to the boundary of the basins of the fixed points E_1 and E_2.

In Fig. 11 it is evident that some portions of the hyperbola δ_s are included inside $A(1)$, and this is consistent with the fact that the chaotic area $A(1)$ is unbounded, as already remarked in the previous sections.

The property that the boundaries of the chaotic area are formed by segments of critical curves also holds for $b \neq 1$, when a closed form solution of the recurrence is not known in terms of elementary functions. In order to show the kind of bifurcation that leads to the creation of the unbounded chaotic

area existing for the map (27) with $b = 1$, we consider a value of the parameter b for which the attractor does not contain portions of δ_s, so that it is included inside a bounded absorbing area $A(b)$, and then we gradually change the value of the parameter b until a contact between δ_s and the boundary of $A(b)$, formed by segments of critical curves, occurs.

Our starting value is $b = 0.93$. At this stage a numerically generated trajectory fills up the chaotic area $A(b)$ shown in Fig. 12. As b is increased the chaotic area enlarges until it has a contact with the lower branch of the hyperbola δ_s. This occurs for $b = b_c = 0.933\dots$ [see the enlargement in Fig. 13(a)] and it can be described as a contact between LC and δ_s [see Fig. 13(b)]. After this contact an unbounded attracting set appears, as shown in Fig. 14, obtained with $b = 0.934$.

At the contact between LC and δ_s the chaotic area $A(b)$ is transformed from a bounded one-piece chaotic area into an unbounded chaotic area. It is

worth noticing that also the map T^2 has the same attracting set, i.e. it is not a two-piece (or two-cyclic) attracting set. In order to understand why, at the contact, the upper portion of the chaotic area suddenly appears, it is convenient to consider the restriction (28) of the map T to the invariant diagonal Δ. The graphs of this one-dimensional map before and after the contact bifurcations are shown in Figs. 15(a) and 15(b) respectively. The graph of the function (28) is characterized by two vertical asymptotes, whose abscissas correspond to the two intersections of δ_s with Δ

$$\delta_s \cap \Delta = \left\{ \frac{3 - \sqrt{3}}{4}, \frac{3 + \sqrt{3}}{4} \right\} \tag{33}$$

and by two local extrema, a local maximum point at

$$c_{-1}^M = \frac{1}{4}(4b - 3 - \sqrt{16b^2 - 48b + 33})$$
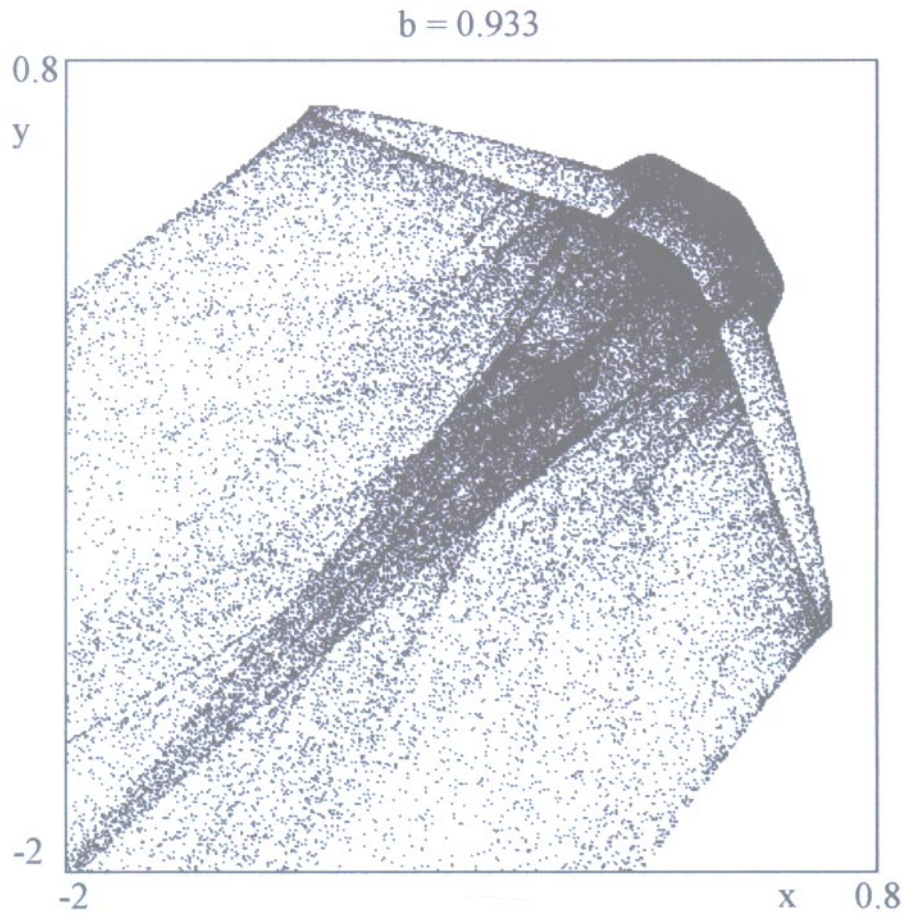
b = 0.933

(a)

Fig. 13.   For $b = 0.933$ the absorbing area is very close to δ_s. (a) Iterated points in the portion of the absorbing area near δ_s. (b) Boundary of the absorbing area, obtained by segments of critical curves, in the region near δ_s.
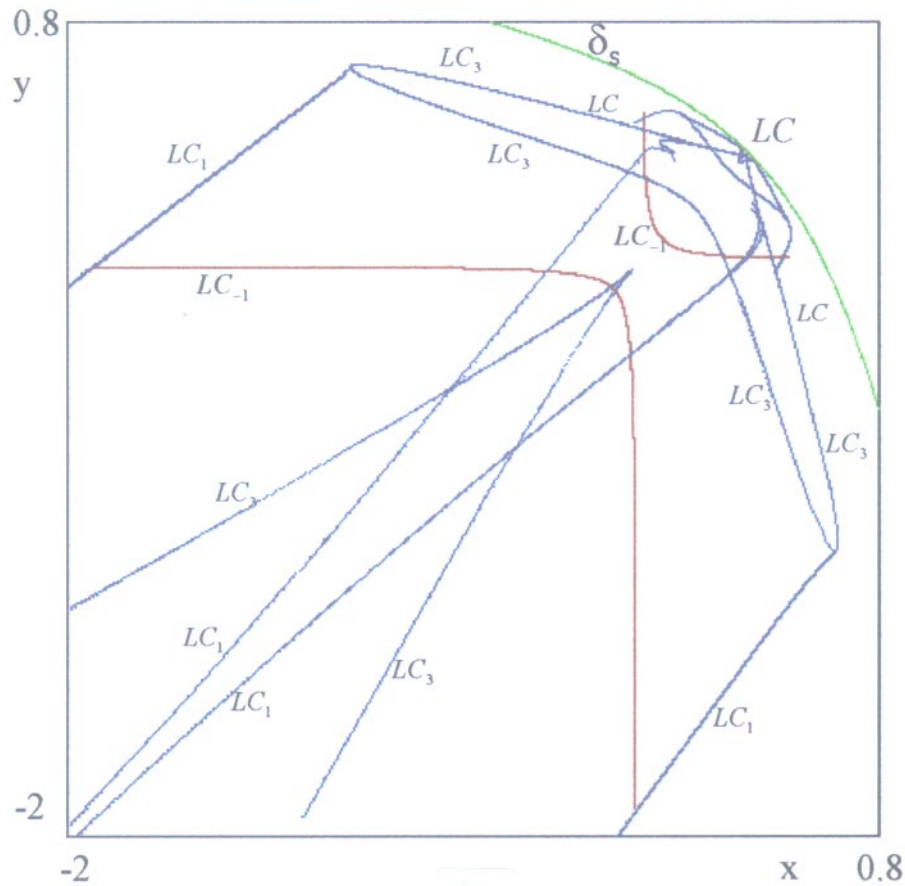
(b)

Fig. 13.   (*Continued*)

and a local minimum at

$$c_{-1}^m = \frac{1}{4}\left(4b - 3 + \sqrt{16b^2 - 48b + 33}\right).$$

There are three fixed points, $p^* < q^* < r^*$: q^* is stable, whereas p^* and r^* are unstable. The basin, along Δ, of the stable fixed point is $B(q^*) = (r_{-1}^*, r^*)$, where $r_{-1}^* = g^{-1}(r^*)$ is the rank-1 preimage of r^* distinct from r^* itself (see Fig. 15). The bifurcation which marks the transition from a one-piece bounded absorbing interval into a two-piece unbounded absorbing interval is due to the merging of the abscissa of the local maximum value $c^M = g(c_{-1}^M)$ with that of the vertical asymptote $x = (3 - \sqrt{3})/4$. In fact, for $b < b_c$ we have $c^M < (3 - \sqrt{3})/4$, and all the trajectories which start with initial conditions out of the basin of q^* enter the absorbing interval

$$I_1 = [c_1^M, c^M] \tag{34}$$

where $c_1^M = g(c^M)$. For $b > b_c$ we have $c^M > (3 - \sqrt{3})/4$, so that the absorbing interval becomes

unbounded, given by

$$I_2 = (-\infty, c^M] \cup [c_1^M, +\infty) \tag{35}$$

with basin

$$B(I_2) = (-\infty, r_{-1}^*] \cup [r^*, +\infty)$$

The absorbing interval I_2 is unbounded because it includes the point $(3 - \sqrt{3})/4 \in \delta_s$. Moreover, it is formed by the union of two pieces because a neighborhood of c^M exists whose points are mapped by g into the interval $((3 - \sqrt{3})/4, r_{-1}^*)$ and then, after another application of g, in the region with $x > r^*$ [see the trajectory whose early points are represented in Fig. 15(b)]. Then the trapping interval I_2 is entered after a finite number of iterations.

The unbounded absorbing interval I_2 exists as far as $c^M < r_{-1}^*$. The bifurcation condition $c^M = r_{-1}^*$ (or equivalently, $c_1^M = r^*$) represents the final bifurcation (or boundary crisis) which leads to the
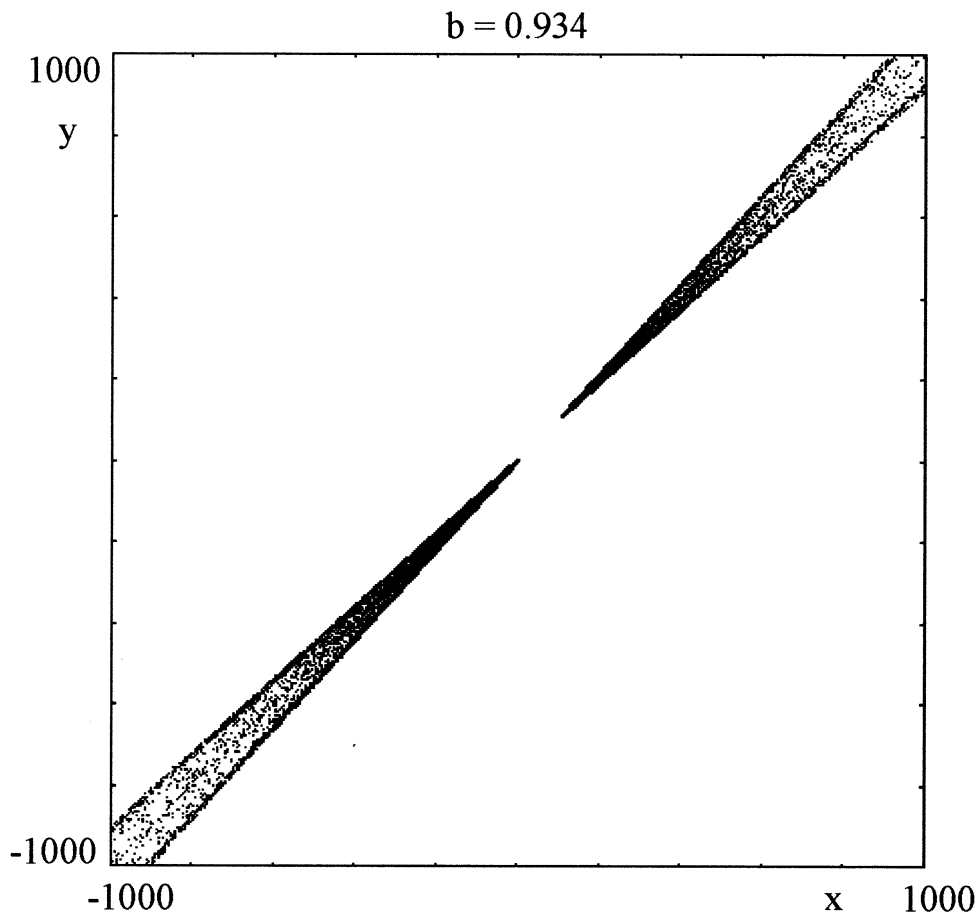
Fig. 14. A trajectory of (27) with $b = 0.934$, just after the contact bifurcation between LC and δ_s. The absorbing area is unbounded, the upper-right and lower-left portions are connected at infinity (on the Poincaré Equator).

(a)

(b)
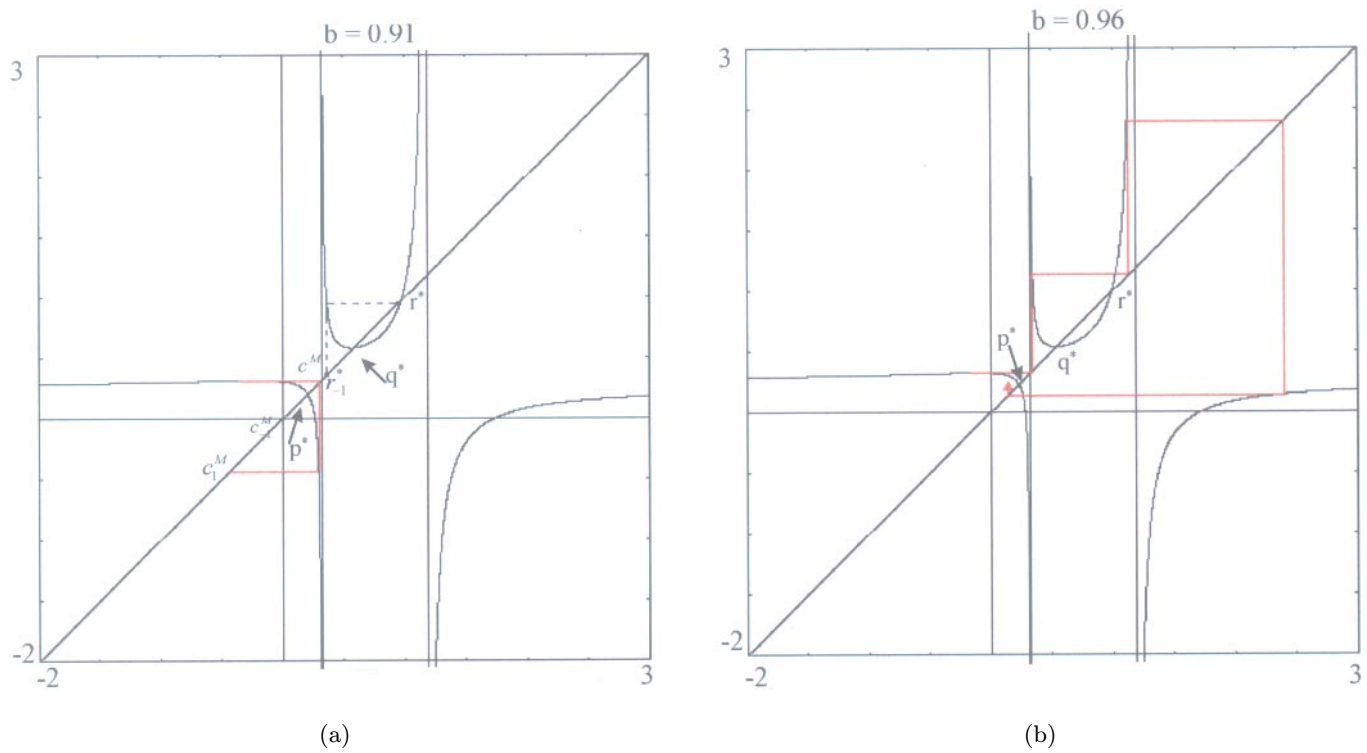
Fig. 15. Graph of the one-dimensional restriction (28) of (27) to the invariant line Δ of equation $x = y$. (a) $b < b_c$; (b) $b > b_c$.
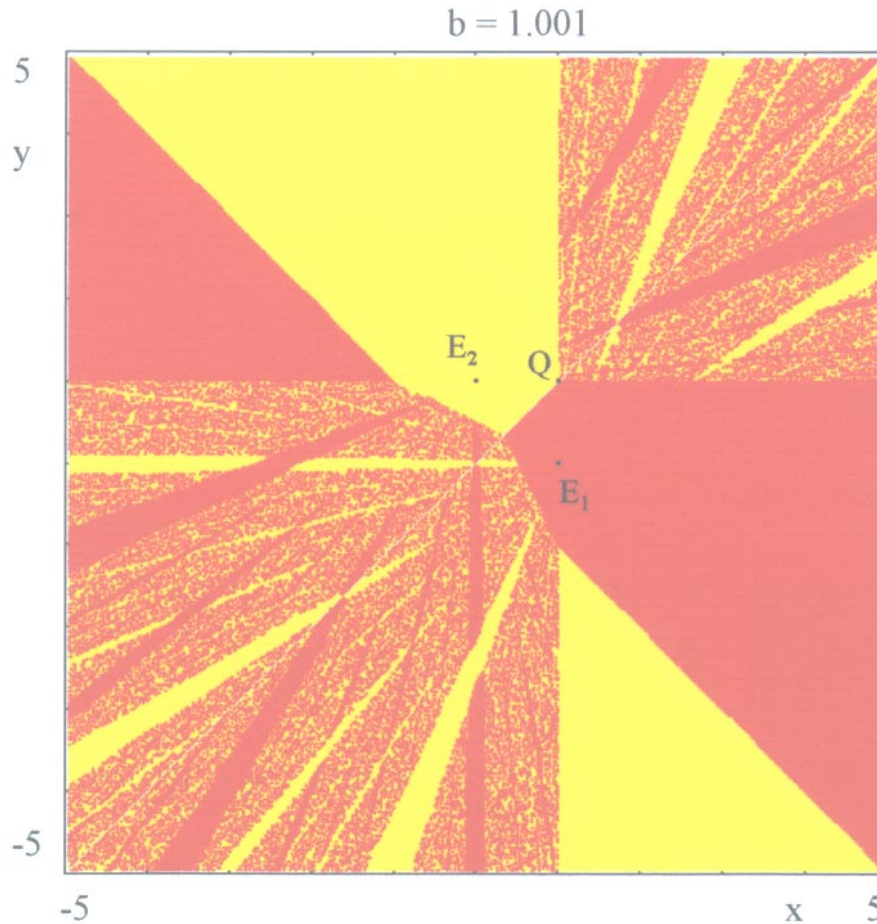
Fig. 16. Basins of the two stable points E_1 and E_2, represented by red and yellow colors respectively, obtained for $b = 1.001$, just after the final bifurcation. At $b = 1$ the whole boundary of the chaotic area merges with the boundary of its basin, so that the usual contact bifurcation between critical curves and basin boundaries does not occur at isolated points, but involves the merging of whole portions of critical segments with segments of basin boundaries.

disappearance of I_2. This occurs at $b = 1$. In fact, for $b = 1$ we have $p^* = 1/4$, $q^* = 1/2$ and $r^* = 1$, together with $c_{-1}^M = 0$, which implies $c^M = g(0) = 1/3$ and $c_1^M = g(1/3) = 1$. For $b > 1$ the generic trajectory embedded inside Δ converges to q^*.

Also for the two-dimensional map (27) $b = 1$ corresponds to the final bifurcation of the chaotic attractor $A(1)$. We remark that at $b = 1$ the whole boundary of the chaotic area, given in (31), merges with the boundary of its basin. In other words, the usual contact bifurcation between critical curves and basin boundaries (see [Mira *et al.*, 1996a]) does not occur at isolated points, but involves a merging of whole portions of critical segments with segments of basin boundaries. After this contact bifurcation the chaotic attractor is transformed into a chaotic repellor, and the generic trajectory converges to one of the stable fixed points, E_1 and E_2, after a chaotic transient. In Fig. 16 the basins of the two

attracting fixed points are shown for $b = 0.001$, just after the final bifurcation of the unbounded chaotic attractor. The fixed point $Q = (q^*, q^*) \in \Delta$ is a saddle point for the two-dimensional map T, with stable set along Δ (and belonging to the boundary between the basins of the two stable fixed points) and unstable set transverse to it.

4.2. From bounded invariant closed curves to an unbounded attractor

As a further two-dimensional example, we consider the map $T : (x, y) \to (x', y')$ defined by

$$
T : \begin{cases} x' = ax + \gamma y + \dfrac{b}{(x + y)^2} - c \\ y' = \alpha x + \beta y \end{cases} \tag{36}
$$
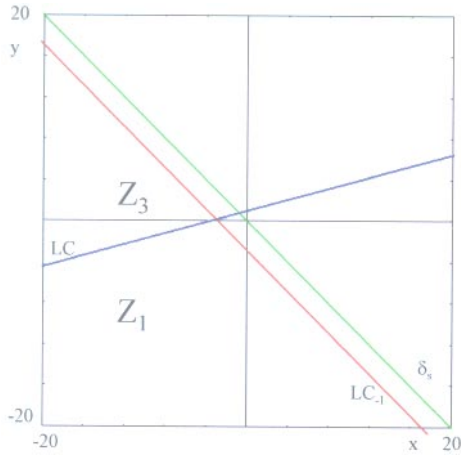
(a)
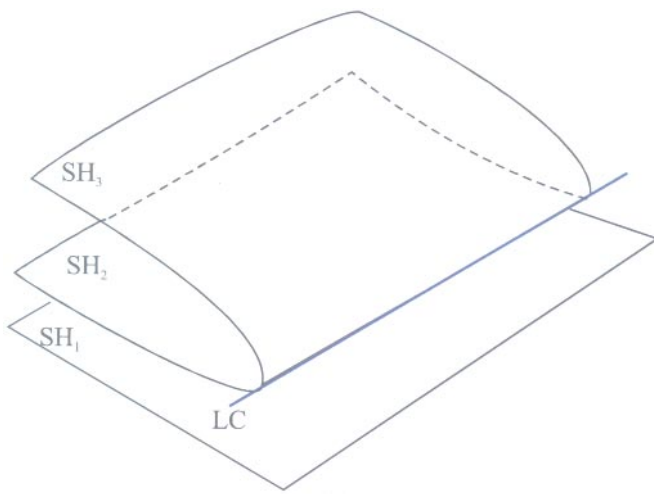
(b)

Fig. 17.   (a) Critical curves LC_{-1} and LC for the map (36), together with the set of nondefinition δ_s. (b) Riemann foliation for the map (36).

whose set of nondefinition is

$$\delta_s = \{(x, y)|x + y = 0\} \qquad (37)$$

As usual, the recurrence obtained by the iteration of the map (36) is well defined provided that the initial condition $(x_0, y_0) \in E$, where E is the trapping set defined in (7).

The map (36) is a noninvertible map of $Z_1 - Z_3$ type. In fact, if we solve the algebraic system (36) to express the variables x and y as functions of x' and y', we get a third degree algebraic system, which may have one or three distinct real solutions. From the condition $\det DT(x, y) = 0$, where
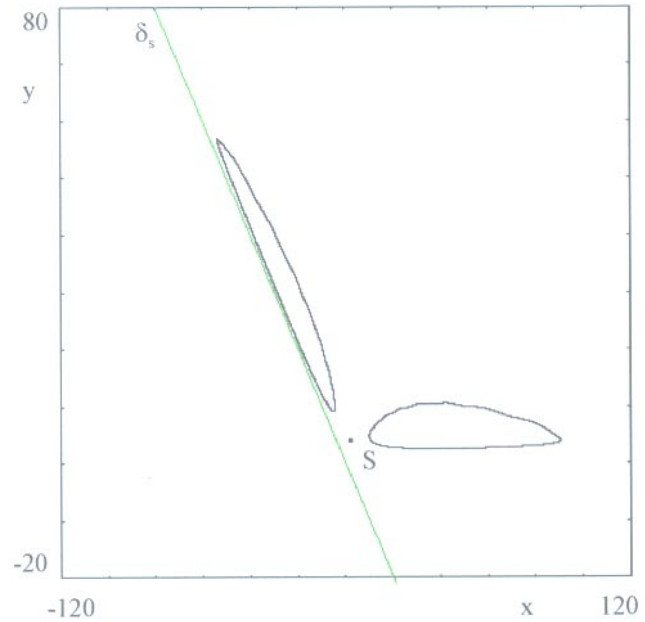
Fig. 18.   A trajectory of the map (36) with $a = -0.6$, $b = 100$, $\gamma = 0.6$, $\beta = 0.7$ and $c = 1.935$, which converges to a two-cyclic attractor. The fixed point S, located between the two-cyclic attracting closed curves, is a saddle point.

$$DT(x, y) = \begin{bmatrix} a - \dfrac{2b}{(x+y)^3} & \gamma - \dfrac{2b}{(x+y)^3} \\ \alpha & \beta \end{bmatrix}$$

the equation of the critical curve of rank-0 LC_{-1} is readily obtained

$$y = -x + \sqrt[3]{\dfrac{2b(\alpha - \beta)}{\alpha\gamma - a\beta}} \qquad (38)$$

i.e. LC_{-1} is a line parallel to δ_s. It is immediate to see that the critical curve of rank-1, $LC = T(LC_{-1})$, is the line of equation

$$y = \frac{\alpha - \beta}{a - \gamma}x + \frac{\alpha - \beta}{a - \gamma}$$

$$\times \left(c - \gamma\sqrt[3]{\frac{2b(\alpha - \beta)}{\alpha\gamma - a\beta}} - \frac{\alpha\gamma - a\beta}{2(\alpha - \beta)}\right)$$

$$+ \beta\sqrt[3]{\frac{2b(\alpha - \beta)}{\alpha\gamma - a\beta}} \qquad (39)$$

The three lines δ_s, LC_{-1} and LC are shown in Fig. 17(a). The line LC separates the plane into two regions: the points belonging to the region below LC, denoted by Z_1 in Fig. 17, have one rank-1 preimage, and the points belonging to the region
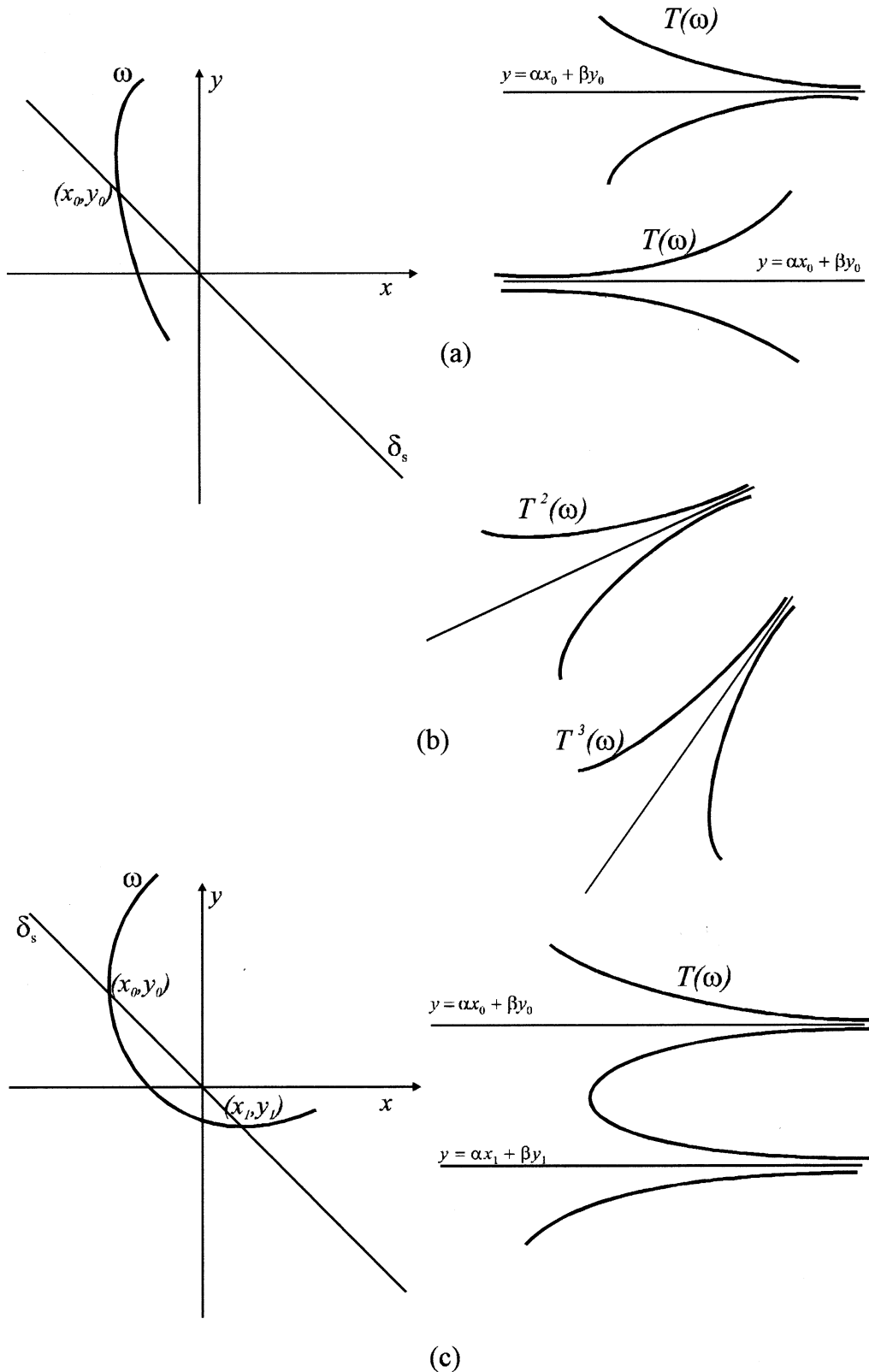
Fig. 19.   Qualitative picture to show how an arc ω, which crosses the line of nondefinition δ_s, is transformed by one or more applications of the map (36). (a) On the left an arc ω is shown which crosses δ_s at one point, (x_0, y_0), and on the right two possible images $T(\omega)$ are shown, constituted by unbounded arcs asymptotic to the line $x = \alpha x_0 + \beta y_0$. (b) Curves obtained by further applications of T, given by $T(\omega)$ and $T^2(\omega)$ respectively. (c) If ω crosses the curve δ_s at two points, (x_0, y_0) and (x_1, y_1), then its image $T(\omega)$ is made up of three branches, an example is given by the qualitative sketch shown on the right.

above LC, denoted by Z_3 in Fig. 17, have three distinct rank-1 preimages. We may say that three distinct inverses T_i^{-1}, $i = 1, 2, 3$, are defined in the region Z_3, whereas only one inverse, T_1^{-1}, exists in the region Z_3. This may be visualized by the Riemann foliation of the plane (see [Mira *et al.*, 1996b] or [Mira *et al.*, 1996a, Chap. 3]) where each inverse mapping T_i^{-1} is considered as defined in a different sheet SH_i [see Fig. 17(b)]. The two sheets SH_1 and SH_2 only exist in the region Z_3, and they join along a fold represented by the critical curve LC, where the preimages obtained by the two inverses T_1^{-1} and T_2^{-1} merge and disappear. On the basis of the structure of the Riemann foliation, we may say that the map (36) is, in some sense, a two-dimensional extension of the one-dimensional map (19), whose foliation is simply given by its graph (see Fig. 5).

We now illustrate a contact bifurcation which leads to the creation of an unbounded set of attraction for the recurrence obtained by the iteration of

the map (36). We start from the situation shown in Fig. 18, obtained with $a = -0.6$, $b = 100$, $\gamma = 0.6$, $\beta = 0.7$ and $c = 1.935$, where the generic trajectory converges to an attractor, say A, belonging to period-two invariant closed curves, created via a supercritical Neimark–Hopf bifurcation of a cycle of period two, on which the asymptotic dynamics are either periodic or quasiperiodic, depending on a rotation number rational or irrational respectively. The fixed point S, located between the two-cyclic attracting orbits, is a saddle point. It can be noticed that the attractor A is very close to the line of nondefinition δ_s. If the parameter c is increased with respect to the value used to obtain Fig. 18, the attractor A has a contact with δ_s.

On the basis of the results given in Sec. 2, we try to understand what will happen after the first contact between A and δ_s. Let us suppose that an arc $\omega \in A$ crosses δ_s at a point (x_0, y_0) [Fig. 19(a)]. Then its image $T(\omega)$ must include two unbounded arcs, asymptotic to the horizontal line
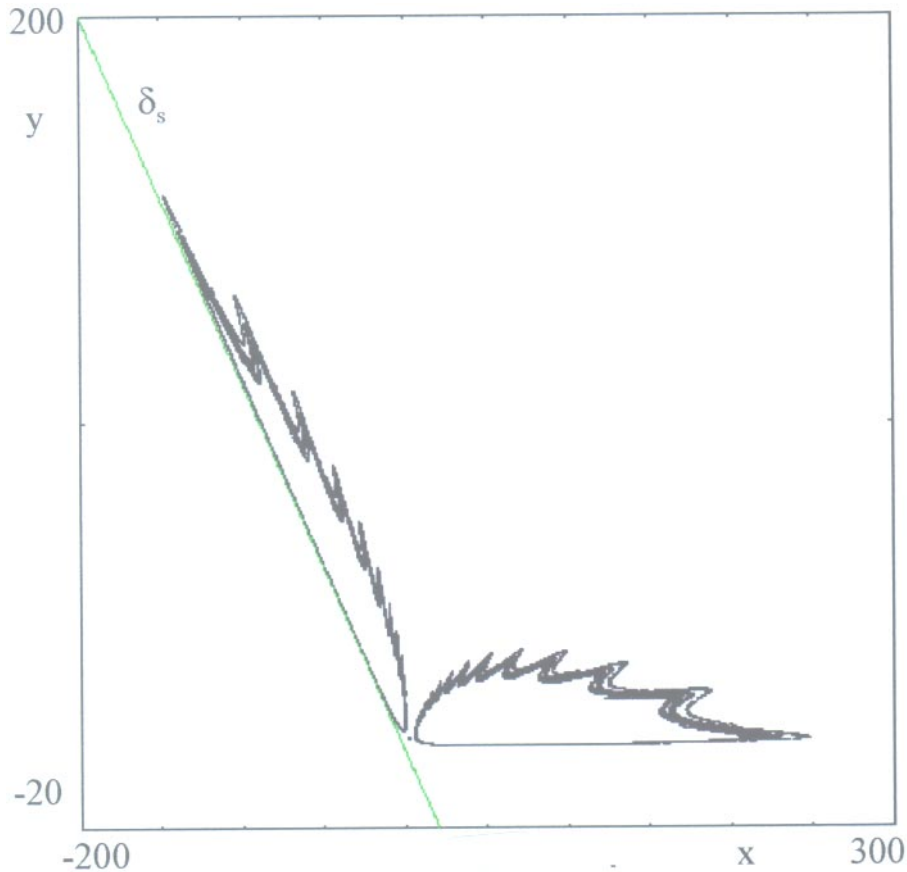
(a)

Fig. 20. (a) A trajectory of the map (36) with $a = -0.6$, $b = 100$, $\gamma = 0.6$, $\beta = 0.7$ (the same as in Fig. 18) and $c = 2$. (b) A trajectory of the map (36) with $a = -0.6$, $b = 100$, $\gamma = 0.6$, $\beta = 0.7$ [the same as in (a)] and $c = 2.1$.
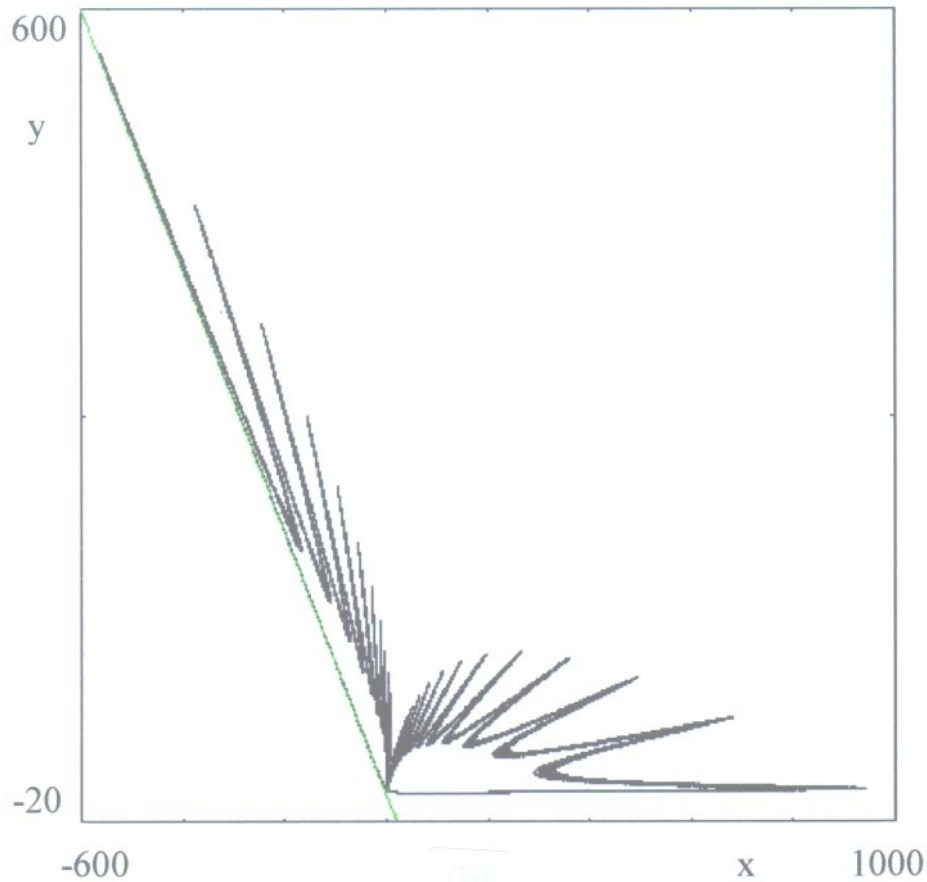
(b)

Fig. 20. (*Continued*)

$$y = \alpha x_0 + \beta y_0. \qquad (40)$$

In fact, as $(x, y) \to (x_0, y_0)$ along ω, we have

$$\lim_{(x,y)\to(x_0,y_0)} T(\omega) = (\pm\infty, \alpha x_0 + \beta y_0)$$

where $+\infty$ is obtained if $b > 0$ and $-\infty$ is obtained if $b < 0$ [see Fig. 19(a)]. Thus, if A crosses δ_s in (x_0, y_0) then it necessarily includes at least two unbounded arcs asymptotic to the line (40). Furthermore, A must also include $T^2(\omega)$ which contains unbounded arcs as well, asymptotic to $T(\{y = \alpha x_0 + \beta y_0\})$, which, for sufficiently high values of $|x|$, is well approximated by the line

$$y = \frac{\alpha}{a}x + H(x_0, y_0) \qquad (41)$$

where $H(x_0, y_0)$ is a constant depending on the point (x_0, y_0). Of course, if $T(\omega)$ crosses δ_s, say at a point (x_1, y_1), then $T^2(\omega)$ includes other unbounded arcs, asymptotic to the horizontal line $y = \alpha x_1 + \beta y_1$. Analogously, $T^3(\omega)$ must include

unbounded arcs asymptotic to the image of the line (41), which for high values of $|x|$ is close to the line

$$y = \alpha \left(\frac{a + \beta}{a^2 + \gamma\alpha} \right) x + L(x_0, y_0) \qquad (42)$$

and so on [see Fig. 19(b)]. An interesting case is obtained if the arc ω crosses δ_s at two points, as shown in Fig. 19(c). In this case, $T(\omega)$ is asymptotic to two distinct horizontal lines, of equations $y = \alpha x_0 + \beta y_0$ and $y = \alpha x_1 + \beta y_1$, as shown in Fig. 19(c) for the case $b > 0$.

These considerations should help to understand the sequence of numerical iterations shown in Figs. 20 and 21, obtained with increasing values of the parameter c. In Figs. 20(a) and 20(b), obtained with $c = 2$ and $c = 2.1$ respectively, we can see that as the chaotic attractor A approaches δ_s the "germs" of the asymptotes, which will appear inside A after the contact, are growing

up. Figure 21(a) is obtained for $c = 2.3$, just after the contact. The structure of the attracting set A is now characterized by the presence of unbounded arcs which are asymptotic to the lines of the type (41), (42)..., images of the horizontal line of the type (40), visible on the right. The shape of the phase curves which form A clearly shows that, after the contact, at least two intersections between A and δ_s exist. In Fig. 21(b) a much larger view of the unbounded attracting set A is shown.

The unbounded attracting set persists for a wide range of parameters: In Fig. 22 a trajectory is shown, obtained numerically with a higher value of the parameter c, $c = 2.7$. The red region visible in Figs. 21 and 22 represents the basin of attraction of a stable fixed point, which has been created, together with an unstable one, via a fold bifurcation.

5. Conclusions

In this paper we have shown, through theoretical arguments and examples, that unbounded chaotic trajectories are naturally met in the study of iterated maps with a denominator which can vanish. Such trajectories densely cover an unbounded set, but they do not diverge.

In this paper we have given, besides the theoretical arguments which are at the basis of the existence of unbounded chaotic attractors, some examples of unbounded chaotic trajectories and we have described some contact bifurcations which cause the transition from bounded asymptotic dynamics to unbounded (but not diverging) dynamics, both in one-dimensional and two-dimensional fractional maps. The contact bifurcations which mark the transformation of a bounded attracting

(a)
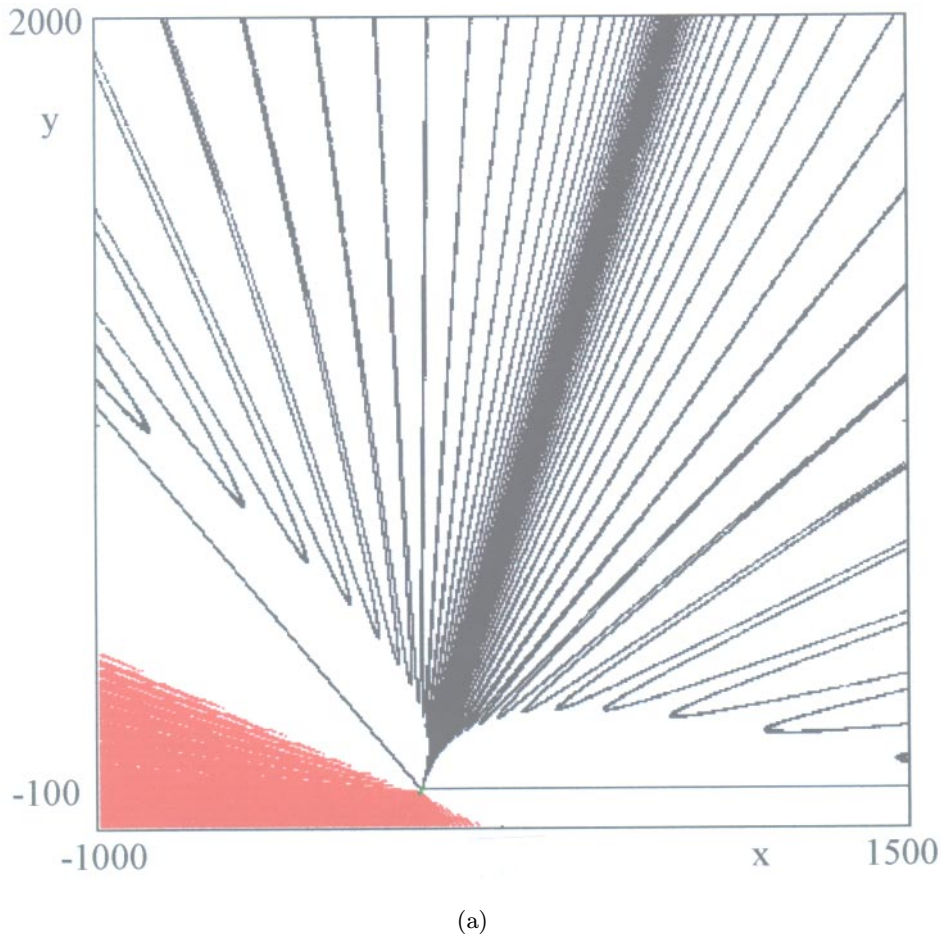
Fig. 21. (a) A trajectory of the map (36) with $a = -0.6$, $b = 100$, $\gamma = 0.6$, $\beta = 0.7$ (the same as in Fig. 20) and $c = 2.3$, just after the contact with δ_s. The structure of the attracting set A is characterized by the presence of unbounded arcs which are asymptotic to the lines of the type (41), (42)..., images of the horizontal line of the type (40), visible on the right. The red region represents the basin of attraction of a stable fixed point, which has been created, together with an unstable one, via a fold bifurcation. (b) A larger view of the trajectory shown in (a).
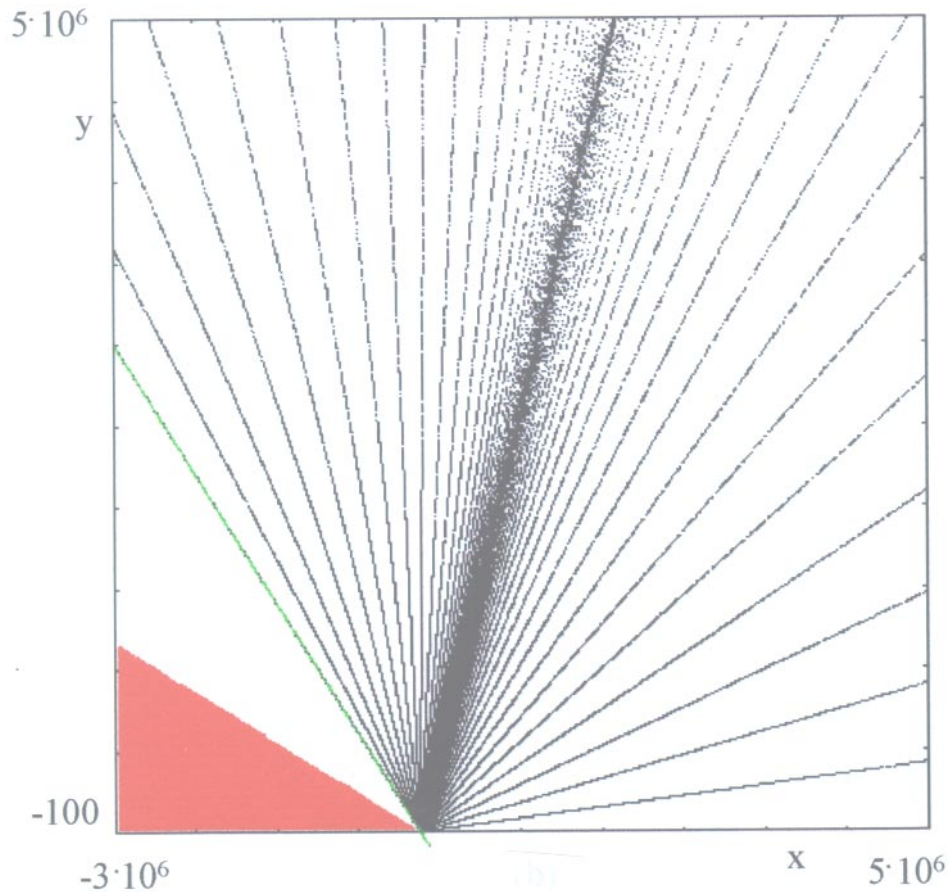
(b)

Fig. 21. (*Continued*)

set into an unbounded one have been studied by the definition of a new kind of singularity, called set of nondefinition and denoted by δ_s, defined as the locus of points where at least one denominator vanishes. For noninvertible maps, such bifurcations can often be described as contacts between critical curves (or critical points, in the case of one-dimensional maps) and the set of nondefinition (which is simply given by the abscissas of the vertical asymptotes in the case of one-dimensional maps).

Two of the examples proposed throughout the paper are given by particular recurrences, obtained by a method based on the Schröder functional equation, for which a closed analytical expression of the unbounded chaotic trajectories can be written in terms of elementary functions.

Many other interesting situations which characterize the dynamics and the global bifurcations of maps with denominator may be related to the presence of δ_s. Some of these phenomena have

been studied in [Bischi *et al.*, 1999a], where it is shown that a contact between the unstable set of a saddle fixed point (or a saddle cycle) and the set of nondefinition may cause the sudden creation of unbounded branches of the unstable set, thus giving a new mechanism for the occurrence of homoclinic bifurcations, specific to maps with a vanishing denominator.

Other interesting situations may arise when an attractor with a bounded basin approaches δ_s as some parameter is varied. In such a case, the contact between the boundary of the attractor and δ_s is necessarily preceded by a contact between the basin boundary and δ_s. At this contact the basin becomes unbounded, and this may give rise to an unbounded chaotic transient before the convergence to the bounded attractor. This dynamic behavior may sometimes reveal that a second global bifurcation is going to occur as the parameter is further varied, due to a contact between the attractor and δ_s. These and other situations related to the
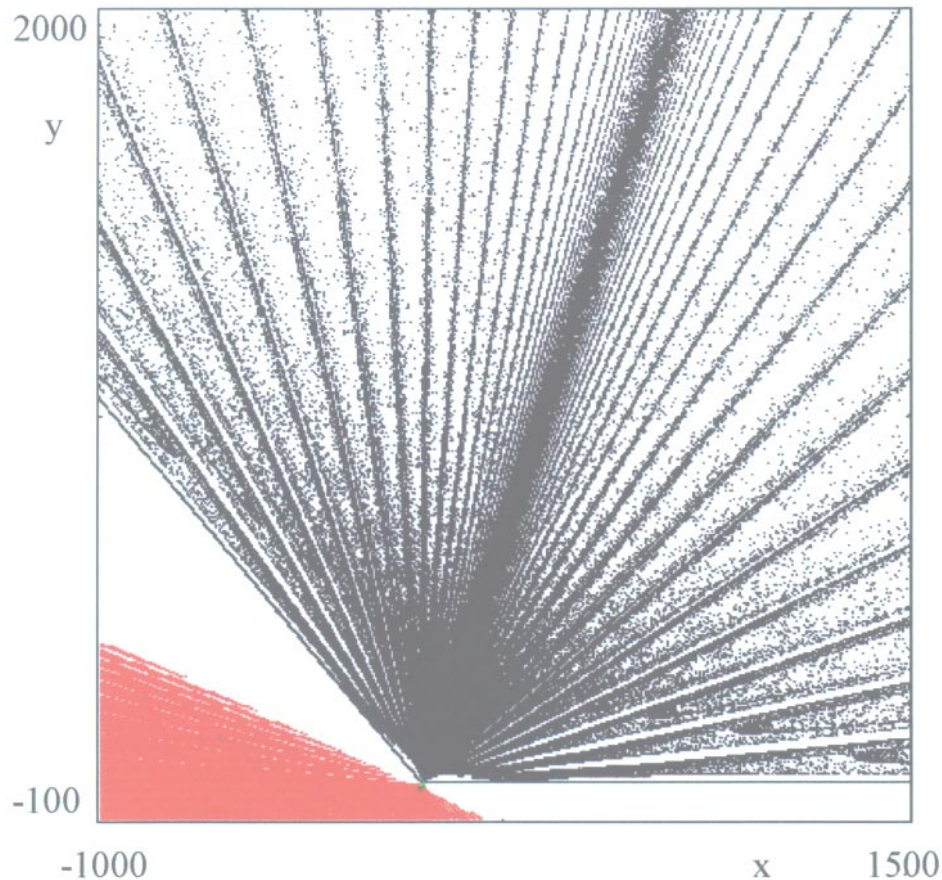
Fig. 22.   A trajectory of the map (36) with $a = -0.6$, $b = 100$, $\gamma = 0.6$, $\beta = 0.7$ (the same as in Fig. 21) and $c = 2.7$.

presence of the set of nondefinition will be the object of further studies.

References

Abraham, R., Gardini, L. & Mira, C. [1997] *Chaos in Discrete Dynamical Systems. A Visual Introduction in Two Dimensions* (Springer-Verlag).

Billings, L. & Curry, J. H. [1996] "On noninvertible maps of the plane: Eruptions," *Chaos* **6**, 108–119.

Billings, L., Curry, J. H. & Phipps, E. [1997] "Lyapunov exponents, singularities, and a riddling bifurcation," *Phys. Rev. Lett.* **6**, 1018–1021.

Billings, L., Curry, J. H. & Phipps, E. [1998] "Symmetric functions and exact Lyapunov exponents," *Physica* **D121**, 44–64.

Bischi, G. I. & Gardini, L. [1997] "Basin fractalization due to focal points in a class of triangular maps," *Int. J. Bifurcation and Chaos* **7**(7), 1555–1577.

Bischi, G. I., Gardini, L. & Mira, C. [1999a] "Maps with denominator. Part 1: Some generic properties," *Int. J. Bifurcation and Chaos* **9**(1), 119–153.

Bischi, G. I., Gardini, L. & Mira, C. [1999b] "Unbounded not diverging trajectories in maps with a vanishing denominator," *Annales Mathematical Silesianae* **13**, 91–102.

Bischi, G. I. & Naimzada, A. [1997] "Global analysis of a nonlinear model with learning," *Economic Notes* **26**(3), 143–174.

Brown, R. & Chua, L. O. [1996] "Clarifying chaos: Examples and counterexamples," *Int. J. Bifurcation and Chaos* **6**(2), 219–249.

Curry, J. H., Garnet, L. & Sullivan, D. [1983] "On the iteration of a rational function: Computer experiments with Newton's method," *Comm. Math. Phys.* **91**, 267–277.

Gardini, L., Bischi, G. I. & Fournier-Prunaret, D. [1999] "Basin boundaries and focal points in a map coming from Bairstow's method," *Chaos* **9**(2), 367–380.

Katok, A. & Hasselblatt, B. [1995] *Introduction to the*

Modern Theory of Dynamical Systems (Cambridge University Press).

Lattès, S. [1906] "Sur les équations fonctionelles qui définissent une courbe ou une surface invariante par une transformation," *Annali di Matematica*, Serie III, Tomo XIII, 1–137.

Marimon, R. & Sunder, S. [1994] "Expectations and learning under alternative monetary regimes: An experimental approach," *Econ. Th.* **4**, 131–162.

Mira, C. [1982] "Equation de Schroeder et solutions des recurrences. Generalisation des polynomes de Tchebycheff," *Proc. Théorie de l'Iteration et ses Applications*, Toulose 1982 (Editions CNRS, Paris), p. 35–43.

Mira, C. [1987] *Chaotic Dynamics* (World Scientific, Singapore).

Mira, C., Gardini, L., Barugola, A. & Cathala, J. C. [1996a] *Chaotic Dynamics in Two-Dimensional Non-invertible Maps* (World Scientific, Singapore).

Mira, C., Carcasses, J.-P., Millerioux, G. & Gardini, L. [1996b] "Plane foliation of two-dimensional non-invertible maps," *Int. J. Bifurcation and Chaos* **6**(8), 1439–1462.

Robinson, C. [1995] *Dynamical Systems* (CRC Press).

Targonski, G. [1981] *Topics in Iteration Theory* (Vandenhoeck & Ruprecht, Gottingen).

Wiggins, S. [1990] *Introduction to Applied Nonlinear Dynamical Systems and Chaos* (Springer-Verlag).

Yee, H. C. & Sweby, P. K. [1994] "Global asymptotic behavior of iterative implicit schemes," *Int. J. Bifurcation and Chaos* **4**(6), 1579–1611.

Appendix A

One-dimensional recurrence obtained by Schröder functional equation

The Schröder functional equation

$$\varphi[f(x)] = \lambda\varphi(x) \qquad (A.1)$$

has an important role in many different fields of mathematics (see e.g. [Lattès, 1906] or [Targonski, 1981]). The use of such functional equation for the determination of recurrences of the form

$$x_{n+1} = f(x_n) \qquad (A.2)$$

having a solution written by a closed form expressed in terms of elementary functions, has been described, both from an historical and a practical point of view in [Gumowski & Mira, 1980], see also [Mira, 1987; Mira *et al.*, 1996]. We recall here the essential steps necessary to obtain the map (23).

Given a function φ, we consider the recurrence (A.2) with the function

$$f(x) = \varphi^{-1}(\lambda\varphi(x)) \qquad (A.3)$$

where φ^{-1} is an inverse of φ. Then Eq. (A.1) becomes

$$\varphi[x_{n+1}] = \lambda\varphi(x_n)$$

which, given an initial condition x_0, becomes

$$\varphi[x_n] = \lambda^n\varphi(x_0)\,.$$

This allows one to write by using the inverse φ^{-1}, the following closed form solution of the recurrence (A.2) with map f given by (A.3)

$$x_n = \varphi^{-1}[\lambda^n\varphi(x_0)]\,. \qquad (A.4)$$

This method allows one to build up recurrences with chaotic solutions if the function φ is given by

$$\varphi(x) = P^{-1}[g(x)]$$

where $P : \mathbb{R} \to [a,\,b]$ is a periodic function and $g : I \to [a,\,b]$, with $I \subseteq \mathbb{R}$.

We now apply this method to obtain the function (23). Let

$$g(x) = \frac{x}{1-x} \quad \text{and} \quad P(x) = \cos x \qquad (A.5)$$

The function φ and its inverse φ^{-1} are defined as

$$\varphi(x) = P^{-1}(g(x)) = \arccos\left(\frac{x}{x-1}\right)$$

with $x \le 1/2$, so that $g(x) \in [-1,\,1]$, and

$$\varphi^{-1}(x) = g^{-1}(P(x)) = \frac{\cos x}{\cos x + 1}$$

with $g^{-1}(u) = u/(u+1)$.

Then the function f can be obtained according to (A.3). If we choose $\lambda = 2$ we get

$$f(x) = \varphi^{-1}(2\varphi(x)) = \frac{\cos\left(2\arccos\dfrac{x}{1-x}\right)}{1 + \cos\left(2\arccos\dfrac{x}{1-x}\right)}$$

$$= \frac{2\cos^2\left(2\arccos\dfrac{x}{1-x}\right) - 1}{2\cos^2\left(2\arccos\dfrac{x}{1-x}\right)}$$

$$= \frac{2\dfrac{x^2}{(1-x)^2} - 1}{2\dfrac{x^2}{(1-x)^2}} = \frac{x^2 + 2x + 1}{2x^2}$$

and the solution (A.4) coincides with (25) with $C = \varphi(x_0)$. The same map f is obtained if we consider $P(x) = \cosh(x)$ with $x \in (1/2, 1)$, so that $g(x) \in [1, +\infty)$. This gives the solution (26).

Appendix B

Two-dimensional recurrence obtained by Schröder functional equation

The method outlined in the Appendix A can be extended to obtain two-dimensional recurrences with solution written in a closed form and expressed by elementary functions.

Given a vector function $\varphi : \mathbb{R}^2 \to \mathbb{R}^2$ defined as

$$\varphi(x, y) = (\varphi_1(x, y), \varphi_2(x, y)) \qquad \text{(B.1)}$$

we consider the recurrence

$$\varphi(x_{n+1}, y_{n+1}) = (\lambda_1 \varphi_1(x_n, y_n), \lambda_2 \varphi_2(x_n, y_n))$$

which, starting with the initial condition (x_0, y_0), gives

$$\varphi(x_n, y_n) = (\lambda_1^n \varphi_1(x_0, y_0), \lambda_2^n \varphi_2(x_0, y_0)). \qquad \text{(B.2)}$$

This allows one to obtain the closed form solution of the two-dimensional recurrence

$$(x_{n+1}, y_{n+1}) = (f_1(x_n, y_n), f_2(x_n, y_n)) \qquad \text{(B.3)}$$

with

$$(f_1(x, y), f_2(x, y)) = \varphi^{-1}(\lambda_1 \varphi_1(x, y), \lambda_2 \varphi_2(x, y)) \qquad \text{(B.4)}$$

where φ^{-1} is an inverse of the mapping (B.1). On the basis of (B.2), the solution of (B.3) can be written as

$$(x_n, y_n) = \varphi^{-1}(\lambda_1^n \varphi_1(x_0, y_0), \lambda_2^n \varphi_2(x_0, y_0)). \qquad \text{(B.5)}$$

In order to obtain the map (27), whose iteration generates the chaotic sequence (32), we consider the two-dimensional periodic function $P : \mathbb{R}^2 \to [-1, 1] \times [-1, 1]$ given by

$$P(x, y) = (P_1(x, y), P_2(x, y)) = (\cos x, \cos y)$$

and the function $g : \mathbb{R}^2 \to \mathbb{R}^2$ given by

$$g(x, y) = (g_1(x, y), g_2(x, y))$$
$$= \left(\frac{x}{x + y - 1}, \frac{y}{x + y - 1} \right)$$

and we define the function φ as

$$\varphi(x, y) = P^{-1}(g(x, y))$$
$$= \left(\arccos \frac{x}{x + y - 1}, \arccos \frac{y}{x + y - 1} \right) \qquad \text{(B.6)}$$

where the arccos function is, as usual, the inverse of the cosine function that maps the interval $[-1, 1]$ to the interval $[0, \pi]$, so that φ is well defined provided that the range of the function g is included inside $[-1, 1] \times [-1, 1]$, i.e. $(x, y) \in A_1 \cup A_2$, where A_1 and A_2 are given in (31). The inverse φ^{-1} is easily obtained as

$$\varphi^{-1}(x, y) = g^{-1}(P(x, y))$$
$$= \left(\frac{\cos x}{\cos x + \cos y - 1}, \frac{\cos y}{\cos x + \cos y - 1} \right) \qquad \text{(B.7)}$$

with $g^{-1}(u, v) = (u/(u + v - 1), v/(u + v - 1))$.

The two-dimensional map (27) is obtained from (B.4) with φ and φ^{-1} given by (B.6) and (B.7) respectively, and with $\lambda_1 = \lambda_2 = 2$:

$$f(x, y) = \left(\frac{\cos\left(2 \arccos \dfrac{x}{x + y - 1}\right)}{\cos\left(2 \arccos \dfrac{x}{x + y - 1}\right) + \cos\left(2 \arccos \dfrac{y}{x + y - 1}\right) - 1}, \right.$$
$$\left. \frac{\cos\left(2 \arccos \dfrac{y}{x + y - 1}\right)}{\cos\left(2 \arccos \dfrac{x}{x + y - 1}\right) + \cos\left(2 \arccos \dfrac{y}{x + y - 1}\right) - 1} \right)$$

$$
= \left(\frac{2\dfrac{x^2}{(x+y-1)^2} - 1}{2\dfrac{x^2}{(x+y-1)^2} + 2\dfrac{y^2}{(x+y-1)^2} - 3}, \; \frac{2\dfrac{y^2}{(x+y-1)^2} - 1}{2\dfrac{x^2}{(x+y-1)^2} + 2\dfrac{y^2}{(x+y-1)^2} - 3} \right)
$$

$$
= \left(\frac{y^2 + 2xy - x^2 - 2x - 2y + 1}{x^2 + 6xy + y^2 - 6x - 6y + 3}, \; \frac{x^2 + 2xy - y^2 - 2x - 2y + 1}{x^2 + 6xy + y^2 - 6x - 6y + 3} \right)
$$

where the identity $\cos(2\arccos(z)) = 2z^2 - 1$ has been used. The solution (32) is obtained from (B.5) with φ and φ^{-1} given by (B.6) and (B.7) respectively.